LAG3 is not expressed in human and murine neurons and does not modulate α-synucleinopathies.

Marc Emmenegger*[1], Elena De Cecco*[1], Marian Hruska-Plochan*[2], Timo Eninger[3,4], Matthias M. Schneider[5], Melanie Barth[3,4], Elena Tantardini[2], Pierre de Rossi[2], Rebekah G. Langston[6], Alice Kaganovich[6], Andrès Gonzalez-Guerra[1], Merve Avar[1], Daniel Heinzer[1], Regina Reimann[1], Lisa M. Häsler[3,4], Therese W. Herling [5], Naunehal S. Matharu[5], Natalie Landeck[6], Kelvin Luk[7], Ronald Melki[8], Philipp J. Kahle[3,4], Simone Hornemann[1], Tuomas P. J. Knowles[5,9], Mark R. Cookson[6], Magdalini Polymenidou[2], Mathias Jucker[3,4], and Adriano Aguzzi[#1]

[1]Institute of Neuropathology, University of Zurich, CH-8091 Zurich, Switzerland

[2]Department of Quantitative Biomedicine, University of Zurich, CH-8057, Switzerland

[3]German Center for Neurodegenerative Diseases (DZNE), Tübingen, Germany

[4]Department of Cellular Neurology, Hertie Institute for Clinical Brain Research, University of Tübingen, Tübingen, Germany

[5]Centre for Misfolding Diseases, Yusuf Hamied Department of Chemistry, University of Cambridge, Lensfield Road, Cambridge CB2 1EW, United Kingdom

[6]Cell Biology and Gene Expression Section, Laboratory of Neurogenetics, National Institute on Aging, National Institutes of Health, Building 35, Room 1A116, 35 Convent Drive, MSC 3707, Bethesda, MD, 20892-3707, USA

[7]Department of Pathology and Laboratory Medicine and Center for Neurodegenerative Disease Research, University of Pennsylvania Perelman School of Medicine, Philadelphia, PA, 19104, USA

[8]Institut François Jacob (MIRCen), CEA, and Laboratory of Neurodegenerative Diseases, CNRS, Fontenay-aux-Roses, France.

[9]Cavendish Laboratory, Department of Physics, University of Cambridge, JJ Thomson Ave, Cambridge CB3 0HE, United Kingdom

*equal contribution

[#]corresponding author

Abstract

While the initial pathology of Parkinson's disease and other α-synucleinopathies is often confined to circumscribed brain regions, it can spread and progressively affect adjacent and distant brain locales. This process may be controlled by cellular receptors of α-synuclein fibrils, one of which was proposed to be the LAG3 immune checkpoint molecule. Here, we analyzed the expression pattern of LAG3 in human and mouse brains. Using a variety of methods and model systems, we found no evidence for LAG3 expression by neurons. While we confirmed that LAG3 interacts with α-synuclein fibrils, the specificity of this interaction appears limited. Moreover, overexpression of LAG3 in cultured human neural cells did not cause any worsening of α-synuclein pathology ex vivo. The overall survival of A53T α-synuclein transgenic mice was unaffected by LAG3 depletion and the seeded induction of α-synuclein lesions in hippocampal slice cultures was unaffected by LAG3 knockout. These data suggest that the proposed role of LAG3 in the spreading of α-synucleinopathies might not be universally valid.

Introduction

Lymphocyte-activation gene 3 (LAG3) is an inhibitory immune checkpoint molecule. Its antibody-mediated blockade is being investigated as a treatment of solid and hematologic tumors (Nguyen and Ohashi, 2015; Andrews *et al.*, 2017; Ascierto *et al.*, 2017; Lichtenegger *et al.*, 2018; Lim *et al.*, 2020; Rohatgi *et al.*, 2020). LAG3 expression in activated T cells, natural killer cells and dendritic cells is well documented (Triebel *et al.*, 1990; Huard *et al.*, 1994, 1997; Hannier and Triebel, 1999; Workman *et al.*, 2002, 2009; Maçon-Lemaître and Triebel, 2005; Camisaschi *et al.*, 2010), supporting a role in the immune system. it has more recently been proposed that LAG3 may function in the central nervous system (CNS) as a receptor of pathogenic α-synuclein assemblies, which are causally involved in Parkinson's disease (PD). Mice devoid of LAG3 were reported to develop lower levels of phosphorylated α-synuclein than wild-type mice upon inoculation with α-synuclein pre-formed fibrils (PFFs). Furthermore, treatment with anti-LAG3 antibodies attenuated the spread of pathological α-synuclein and drastically lowered the aggregation *in vitro* (Mao *et al.*, 2016).

This finding, if confirmed, could have far-reaching implications. PD is a common neurodegenerative movement disorder (Beitz, 2014; Deweerdt, 2016; Jankovic, 2017), entailing a high level of suffering to the affected patients and their families. Histologically, PD is characterized by α-synuclein aggregates known as Lewy Bodies in neurons of the substantia nigra, whose accumulation is associated with neurodegeneration (Dickson, 2012; Mullin and Schapira, 2015; Corbillé *et al.*, 2016). Growing evidence suggests that α-synuclein fibrils spread from cell to cell (Volpicelli-Daley *et al.*, 2011; Volpicelli-Daley, Luk and Lee, 2014), by a prionoid process of templated conversion (Aguzzi, 2009; Aguzzi and Lakkaraju, 2016; Jucker and Walker, 2018; Kara, Marks and Aguzzi, 2018; Scheckel and Aguzzi, 2018; Uemura *et al.*, 2020). Interrupting transmission of α-synuclein may slow down or abrogate the disease course. Although a more general pathogenic role for LAG3 in the progression of prion disorders has been ruled out (Liu *et al.*, 2018), impairing the binding of α-synuclein fibrils to neuronal LAG3 may still constitute an attractive target for small drugs or immunotherapy of PD.

Here, we have analyzed LAG3 expression and α-synuclein binding in mouse and human model systems. Additionally, we studied the propagation of pre-formed fibrils (PFFs) of α-synuclein in neural stem cell (NSC)-derived neural cultures, in the presence or absence of LAG3. Finally, we have investigated the in vivo role of LAG3 on survival in the A53T transgenic mouse model of Parkinson's disease, with LAG3 knockout (KO), hemizygous or LAG3-wildtype (WT) genotypes. We failed to detect neuronal expression of LAG3 and were unable to establish any role for LAG3 in α-synucleinopathies either *in vitro* and *in vivo*.

Results

Absence of endogenous LAG3 from neuronal cell lines, NSC-derived neural cultures, and human brain samples

Sequence homology between human and mouse LAG3 proteins is less than 70%, which may limit the use of anti-LAG3 antibodies across species. We therefore asked whether available antibodies bind the extracellular domain of human or mouse LAG3. In a simple indirect enzyme-linked immunosorbent assay (ELISA), recombinant human $LAG3_{23-450}$ and mouse $LAG3_{24-442}$ were coated onto wells of a 384-well plate, and binding was assessed with 8 commercially available anti-LAG3 antibodies (**Fig. 1A**). Except for antibody LS-B15026, all antibodies bound only either human or mouse LAG3, suggesting that the epitopes differ between the species. Western Blot analysis confirmed that the mouse monoclonal antibody 4-10-C9 used in (Mao *et al.*, 2016) did not bind human LAG3 either as recombinant protein or overexpressed by lentivirally transduced murine primary cultures, whereas its murine counterpart was detected (**Fig. 1B**).

We thus aimed to identify a human neural cell line that expresses LAG3. In a Western Blot using five different human cell lines, we found bands specific for LAG3 in activated T lymphocytes but not in any of the human glial, neuronal, or control (HEK293T) cell lines (**Fig. 1C**). We then decided to immunoblot human neural stem cell (NSC)-derived differentiated neural cultures, for which we had available concomitant single-cell RNA sequencing (scRNAseq) data (Hruska-Plochan *et al.*, 2021) and immunofluorescence. Western Blotting did not reveal any LAG3-specific bands (**Fig. 1D**) and scRNAseq yielded only minimal counts for the LAG3 transcript, in neurons (N), astrocytes (AST), and mixed glial (MG) cells (**Fig. 1E**), similar to other T cell checkpoints like T cell immunoreceptor with Ig and ITIM domains (TIGIT) or T cell immunoglobulin and mucin domain-containing protein 3 (TIM3 or HAVCR2) and clearly distinct from neuronal or astrocytic markers (**Fig. S1A**). We then speculated that, although the transcriptional profile is indicative of extremely low levels, there may still be some LAG3 expression, undetectable by bulk methodologies like Western Blotting. We therefore performed an immunofluorescence stain on human neural cultures, some of which were transduced with a lentiviral plasmid encoding human LAG3 as a positive control. No endogenous LAG3 could be identified while lentivirally transduced neural cultures showed LAG3 staining with two different antibodies (**Fig. 1F**).

Subsequently, we investigated human brain areas for LAG3 expression. We selected specific brain regions (i.e. substantia nigra and frontal cortex) that are heavily affected in Parkinson's disease in post-mortem brain homogenates, using both activated T lymphocytes and the lymphoepithelial tissue of the tonsil as positive controls, due to their high expression of LAG3. Western Blotting was unable to reveal the presence of LAG3 in human brain samples (**Fig. 1G**).

Finally, we interrogated a single-nucleus (sn) RNAseq human brain dataset that we have recently described (Saez-Atienzar *et al.*, 2021) for LAG3 expression across different cell types. This data is derived from 21 dorsolateral prefrontal cortices from 16 neurologically healthy donors (median age 36 years, range: 16-61 years), male:female ratio = 1:1) and clustered and annotated using known gene expression markers (see Methods and (Saez-Atienzar *et al.*, 2021)). We saw only background expression of *LAG3* in any of 34 identified cell clusters, including 13 clusters of excitatory and 11 subtypes of inhibitory neurons, oligodendrocytes (ODC), oligodendrocyte precursor cells (OPC), microglia (MGL), astrocytes (AST), and endothelial cells (EC) (**Fig. 1H**). Similar results were obtained when examining available scRNAseq and snRNAseq datasets from juvenile and adult human brain tissue samples including substantia nigra (Zhang *et al.*, 2016; Welch *et al.*, 2019; Agarwal *et al.*, 2020). These results indicate that we were unable to detect LAG3 expression in human neurons using snRNAseq.

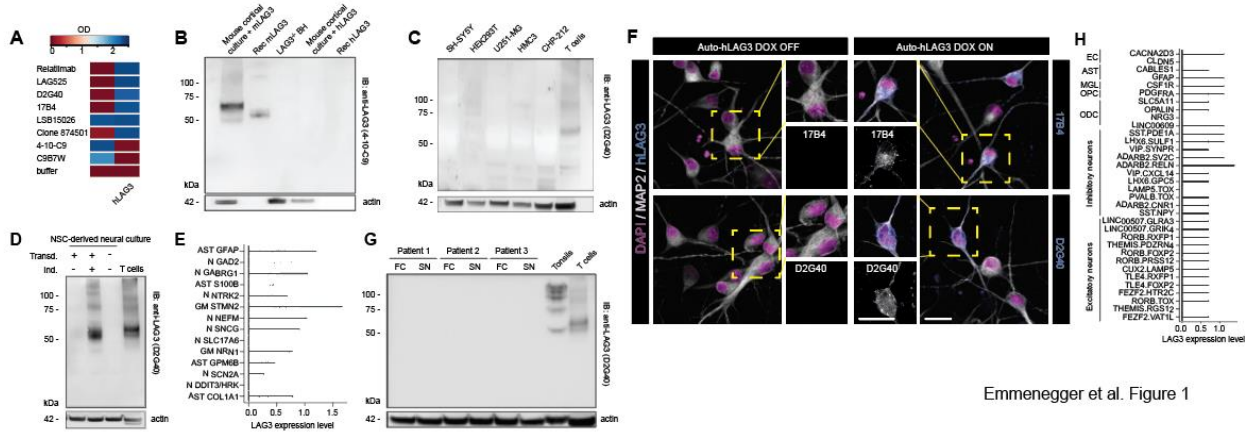

Fig. 1. Absence of expression of LAG3 in human brain cells. **A**. Binding of eight commercial antibodies to recombinant human LAG323-450 and murine LAG324-442 via indirect ELISA. Seven out of eight antibodies bound either human or mouse LAG3, while one antibody (LSB15026) recognized both species. **B**. Specific detection of murine but not human LAG3 using 4-10-C9 anti-LAG3 antibody is confirmed with Western Blotting. **C**. No detection of human LAG3 in neuronal or glial cell lines of human origin. The band for LAG3 was detected in activated T cells. **D**. No band for human LAG3 could be detected with Western Blot in lysates of fully differentiated human NSC-derived neural cultures. **E**. Violin plot showing the RNA expression levels of human LAG3 in human NSC-derived neural cultures. Identities annotate different clusters: Neuronal clusters are comprised of the following markers: GAD2, GABRG1, NTRK2, NEFM, SNCG, SLC17A6, SCN2A, DDIT3/HRK. Mixed glial clusters are defind by the following markers: GFAP, S100B, STMN2, NRN1, GPM6B, COL1A1, with astrocyte-specific clusters characterised by GFAP, S100B, GPM6B, COL1A1. LAG3 cannot be evidenced in any of the clusters beyond few random events. **F**. Using high power, high resolution laser scanning confocal microscopy, no human LAG3 signal could be detected in human neurons (Auto-hLAG3 transduced, DOX OFF) by two different anti-human LAG3 antibodies (17B4 and D2G40; left panel and zoomed-in insets) whereas LAG3 was clearly detected in human neurons induced to express hLAG3 (DOX ON; right panel and zoomed-in insets). Scale bars 25 µm. **G**. Human brain homogenates from autopsy material were immunoblotted for the presence of LAG3. No band for LAG3 could be evidenced in any of the brain homogenates. Control samples (tonsils and activated human T cells) show expected bands. **H**. Nuclei were isolated from 21 human dorsolateral prefrontal cortices from 16 donors, isolated, and were subjected to snRNAseq. Expression levels were quantified and are shown as violin plots. The LAG3 transcripts are non-detectable in all 34 distinct cell types, including multiple excitatory and inhibitory neurons, oligodendrocytes (ODC), oligodendrocyte precursor cells (OPCs) microglia (MGL), astrocytes (AST), or endothelial cells (EC). Cluster markers as detailed in Saez-Atienzar et al. 2021.

Absence of endogenous LAG3 in murine brain samples

As the inability to detect LAG3 in human neuronal samples seemed to contradict previous observations (Mao *et al.*, 2016), we analyzed LAG3 expression in mouse brains. Prior RNAseq data reported that *Lag3* is poorly expressed in both hippocampus and cerebellum of WT mice (Liu *et al.*, 2018), and likely absent in murine neurons (Zhang *et al.*, 2014). Western Blot of total brain homogenates from C57BL/6J wild-type mice did not show any robust LAG3-specific band (**Fig. 2A**). Incubation with a different primary anti-LAG3 antibody (**Fig. S1B**) and an IP-enrichment (**Fig. S2A**) confirmed a lack of detection of endogenous LAG3 in wild-type mouse brain homogenates.

Next, we prepared mixed neuroglial and glial cortical cultures from C57BL/6J mice and assessed both *Lag3* mRNA and LAG3 protein expression. The anti-mitotic compound AraC was added to the mixed cortical cultures to enrich for neurons and eliminate glia n (**Fig. 2B**, lower panels). Western Blotting (**Fig. 2B**) or LAG3 sandwich ELISA, where we additionally included murine synaptoneurosome (to account for α-synuclein expression in the synapse) and brain region-specific preparations (**Fig. 2C**), did not reveal any endogenous LAG3 in any of the samples, even after enrichment by immunoprecipitation from 500 µg of total protein (**Fig. S2B**). Immunofluorescence staining of neuronal-enriched primary cultures led to the same results, with LAG3 being detectable only in the lentivirally transduced cultures that were used as positive controls (**Fig. 2D**).

We next quantified *Lag3* mRNA by RT-qPCR (**Fig. 2E**). By interpolation of the threshold cycle (C_T) of each sample into a standard curve, we estimated the presence of around 1-2 transcripts/ng of RNA in mixed cortical cultures and neuron-enriched cultures, whereas in mixed glial cultures *Lag3* mRNA was slightly more abundant (4-5 transcripts/ng of RNA). These values are close to what we observed for a LAG3$^{-/-}$ mouse brain homogenate (1-2 transcripts/ng of RNA) and are indicative that Lag3 expression is spurious. In contrast, around 1600 transcripts/ng of RNA were counted in activated T cells.

To further expand our analyses, we performed scRNAseq of microdissected ventral midbrain and striatum of 1 year old mice (n=17) that included animals given a single striatal injection of either PBS (vehicle) or LPS as previously described (Russo *et al.*, 2019) and assigned major cluster markers in 76'305 cells (**Fig. S2C**)**.** We then specifically investigated transcript levels of murine Lag3, in endothelial cells, several macrophage subtypes (MPH), astrocyte subtypes, red blood cells (RBC), vascular smooth muscle cells (VSMC), neural precursor cells (NPC), microglia subtypes (MGL), oligodendrocyte subtypes (ODC), T cells, neuron subtypes, oligodendrocyte precursor cells (OPC), ependymal cells (Epnd), choroid plexus cells (ChP), and fibroblasts (Fibr) (**Fig. S2D**). Of all identified murine cells, only Transmembrane Protein 119 (TMEM119)-positive microglia had modest expression of Lag3, marginally above background (**Fig. 2F**). Of interest, activation of microglia with lipopolysaccharide (LPS) led to decreased expression of Lag3 in microglia (**Fig. S2E**). However, and consistent with the negative results for

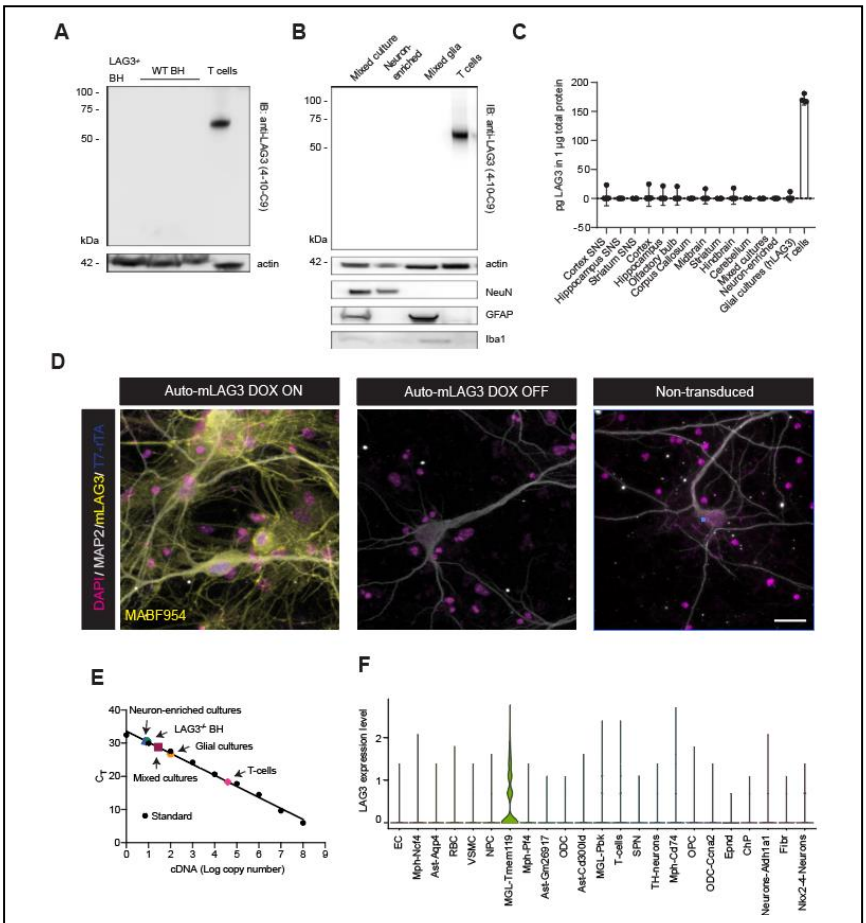

Fig. 2. **Absence of expression of LAG3 in mouse brain cells, particularly in neurons**. **A**. Brain homogenates from LAG3 KO and WT mice were immunoblotted for the presence of murine LAG3. Western Blot does not show a specific band other than for activated murine T cells. **B**. Mixed neuroglial, neuron-enriched, and glial cortical cultures were assayed for the presence of LAG3 where no band could be found. Activated T cells display band at expected size. **C**. Lysates of synaptoneurosomes (SNS) of different brain regions and mouse brain region-specific areas as well as murine activated T cells were assayed for the presence of LAG3 with sandwich ELISA. No evidence for LAG3 could be found in any of the samples other than in activated T cells. Expression is shown in pg LAG3 per µg total protein as mean values of quadruplicates with 95% confidence intervals. **D**. Using high power, high resolution laser scanning confocal microscopy, no mouse LAG3 signal could be detected in murine primary neuronal cultures (Auto-mLAG3 transduced, DOX OFF and non-transduced neurons) using anti-mouse LAG3 antibody (MABF954) whereas LAG3 was clearly detected in primary neurons induced to express mLAG3 (Auto-mLAG3 transduced, DOX ON). Scale bars 20 µm. **E**. RT-qPCR-derived C_T values to measure the cDNA copy number. Mixed neuroglial cultures, glial cultures, and neuron-enriched cultures show transcript levels that are close to indistinguishable to those from LAG3$^{-/-}$ BH. Conversely, around 1600 transcripts/ng of RNA were counted in activated T cells. **F**. Murine mesencephalon and striatum were interrogated with scRNAseq. Violin plot showing expression values of Lag3 between identified cell clusters, mainly expressed in TMEM119-positive microglia cells. Cluster markers are detailed in Russo et al. 2019.

detection of LAG3 in human snRNAseq, we did not detect murine Lag3 in neurons or astrocytes under any condition examined.

Promiscuous binding of α-synuclein fibrils questions selectivity towards LAG3

The above observations suggest that the neuroprotective effects exerted by antibodies to residues 52–109 of the LAG3 D1 domain, or the depletion of LAG3 (Mao *et al.*, 2016), may not be required for the interaction between neuronal LAG3 and α-synuclein fibrils. However, α-synuclein fibrils binding to LAG3 could still be an important component involved in PD by an unknown mechanism. To investigate the interaction between LAG3 and α-synuclein fibrils, we performed ELISA by coating multiple proteins including the human LAG3 structural homologue, CD4 (Triebel *et al.*, 1990; Bae *et al.*, 2014). We then incubated ELISA plates with serial dilutions (highest concentration, using the monomer equivalent: 0.125 µM; lowest concentration: 3 x 10^{-5} µM) of α-synuclein fibrils and filaments of Apoptosis-Associated Speck-like Protein Containing a CARD (ASC). If binding at high enough affinity occurs, the fibrils should be retained by the antigen and could be detected via an antibody. ASC filaments did not bind any of the proteins presented (**Fig. 3A**) but yielded the expected dose-response curves when directly coated onto the plate (**Fig. S3A**). Conversely, α-synuclein fibrils (but not monomeric α-synuclein) interacted with LAG3 although equally so with the microtubule-binding domain (MTBD) of human tau protein, and CD4 (**Fig. 3B**). PrP^{C} , the apolipoprotein E3 (APOE3) as well as TAR DNA-binding protein 43 (TDP-43) were found to interact with lower affinity, whereas bovine serum albumin (BSA), arachis hypogaea 2 (Ara h 2), a major peanut allergen, and uncoated conditions did not display any substantial binding.

Our observations suggest a rather promiscuous binding of α-synuclein fibrils to many proteins including LAG3, MTBD and CD4. We therefore speculated that surface effects may lead to electrostatic interactions. We therefore employed a microfluidics-based technology (Arosio *et al.*, 2016; Scheidt *et al.*, 2019; Schneider *et al.*, 2020) to characterize the receptor ligand interaction via diffusional sizing. Microfluidic diffusional sizing (MDS) measures the hydrodynamic radius (R_h) of a fluorescently labelled protein and can characterize binding by displaying an increase in R_h upon ligand binding. Increasing concentrations of α-synuclein fibrils did not induce a change in the hydrodynamic radius of fluorescently labelled $LAG3_{23-434}$, CD4, or BSA (**Fig. 3C**), whereas a labelled antibody directed against α-synuclein (MJFR1) triggered the expected concentration-dependent size increase. A progressive increase in the concentration of monomeric α-synuclein did not lead to a rise in the hydrodynamic radius of labelled LAG3, however, both anti-LAG3 antibody (Relatlimab) and FGL1, a recently discovered interaction partner of LAG3 (Wang *et al.*, 2019), displayed clear binding (**Fig. 3D**), with affinities of 4.82 ± 0.71 nM and 232 ± 79 nM, respectively. To shed light onto the interaction between α-synuclein fibrils and LAG3, we then decided to additionally perform co-immunoprecipitation experiments. SH-SY5Y cells

overexpressing hLAG3 were incubated with either α-synuclein monomers or fibrils so that the binding could occur on the cell membrane, and then both partners were in turn immunoprecipitated. While immobilized LAG3 only bound α-synuclein fibrils, both monomeric and fibrillar α-synuclein were able to co-precipitate a small fraction of the expressed LAG3 (**Fig. 3E, 3F**). The observation that a major portion of both proteins remains in the unprecipitated soluble fraction further supports that the binding interaction between LAG3 and α-synuclein fibrils is weak.

Membrane-bound LAG3 does not affect the uptake and seeding of α-synuclein PFFs in human neural cultures.

The collective biochemical data presented above led us to question whether there is a physiologically relevant interaction between α-synuclein fibrils and LAG3. Nevertheless, we decided to test its functional relevance in a human cell-based system *in vitro*. We differentiated NSCs into human neural cultures previously shown to be devoid of LAG3 **(Fig. 1D** and **1E**) and transduced them with lentivirus

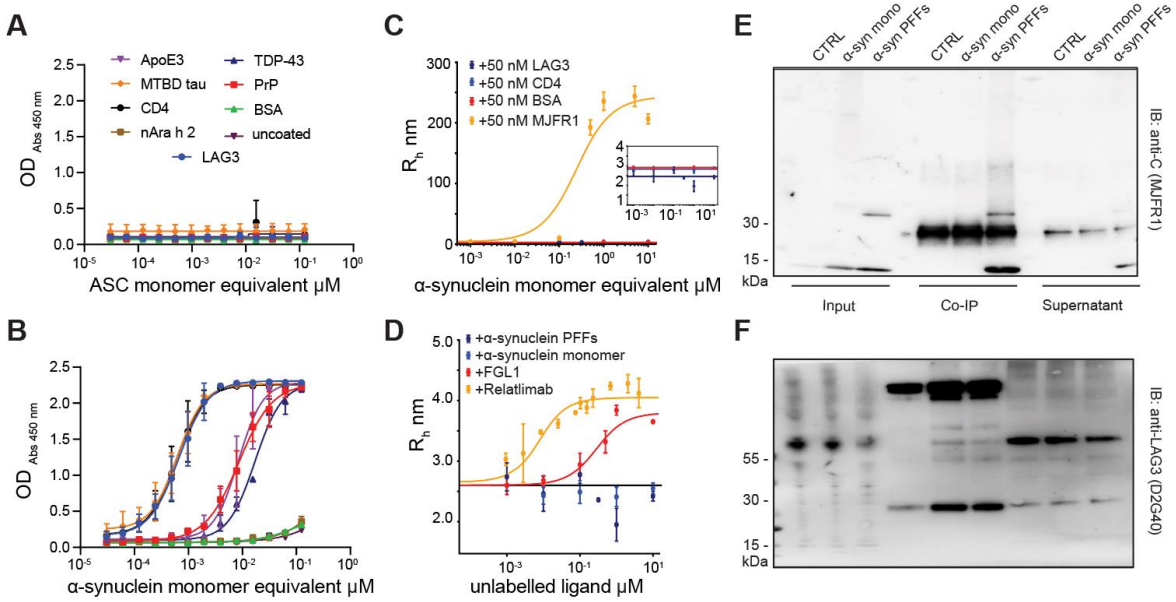

Fig. 3. **Characterization of binding properties between α-synuclein PFFs and LAG3 reveals promiscuous character of α-synuclein**. **A**. and **B**. Binding of ASC filaments (A) or α-synuclein PFFs (B) to multiple proteins. Serial dilutions of ASC filaments and α-synuclein PFFs were performed and bound fractions were detected using anti-ASC or anti-α-synuclein (MJFR1) antibodies. ASC filaments did not interact with any of the proteins (A). Conversely, α-synuclein PFFs strongly bound LAG3, CD4, and MTBD tau and showed moderate binding properties to PrP^C, APOE3, and TDP-43. No binding between α-synuclein PFFs and nAra h 2 or BSA could be detected. Values represent means ± SD of duplicates. **C**. and **D**. Diffusional sizing of α-synuclein PFFs with fluorescently conjugated LAG3, CD4, BSA, and MJFR1 α-synuclein antibody (C) and of fluorescently labelled LAG3 with monomeric α-synuclein, α-synuclein PFFs, FGL1, and Relatlimab anti-LAG3 antibody (D). An increase in the hydrodynamic radius (R_h) of α-synuclein PFFs is seen with increasing concentrations for MJFR1 but not for LAG3 or any of the control proteins, also not at a lower scale (see insert) (C). Similarly, the hydrodynamic radius of labelled LAG3 increases with higher concentrations of Relatlimab and FGL1 but does not change with α-synuclein PFFs or monomeric α-synuclein (D). Values are given as means ± SD of triplicates. **E**. and **F**. Co-immunoprecipitation of LAG3 and subsequent immunoblotting with anti α-synuclein antibody (MJFR1) (E) and co-immunoprecipitation of α-synuclein (monomeric or PFFs) and subsequent immunoblotting with anti-LAG3 antibody (D2G40) (F). Using the anti-α-synuclein antibody for pulldown resulted in LAG3 bands with both monomeric as well as fibrillar α-synuclein. The usage of anti-LAG3 for pulldown led to the specific detection of α-synuclein PFFs, although the PFF fraction predominates also in the input.

encoding for inducible expression of human LAG3. These cultures expressed α-synuclein (**Fig. S4A**). Adapting a published protocol(Volpicelli-Daley, Luk and Lee, 2014), we added sonicated α-synuclein preformed fibrils (PFFs) and incubated the cells them over a period of 14-28 days. Subsequently, we stained the phosphorylated form (pS129) of α-synuclein with two different phosphorylated α-synuclein-specific antibodies. We then compared the amount of α-synuclein fibrils uptake and seeding through intracellular pS129 α-synuclein accumulation, in cultures that did not express (**Fig. S4B**) or expressed **(Fig. S4C**) LAG3. We found no difference in the proportion of cells containing pS129 phospho-α-synuclein between the two conditions, using the 81A (**Fig. 4A**) or EPY1536Y (**Fig. 4B**) anti-pS129 α-synuclein antibodies and LAG3-expressing as well as LAG3 non-expressing neurons infected with α-synuclein PFFs harbored equal amounts of phosphorylated α-synuclein. Quantification of images using a trained ilastik-based algorithm for pixel segmentation evidenced no effect of LAG3 expression **(Fig. 4C, D)**. This suggests no functional role for neuronal LAG3 in the propagation of α-synuclein fibrils in our *in vitro* system.

Overall survival is unchanged in A53T LAG3$^{-/-}$, LAG3$^{+/-}$, or LAG3$^{+/+}$ mice

Human LAG3 may be functionally dissimilar to its murine counterpart suggesting that despite the above negative data there may be an effect of Lag3 in mice systems. Using a well characterized model of α-synucleinopathy, the A53T human α-synuclein mouse model under the mouse Thy1.2 promoter (Van Der Putten *et al.*, 2000), we aimed to examine the effect of LAG3 expression on overall survival. As expression of endogenous α-synuclein is a key requirement for the propagation model (Volpicelli-Daley, Luk and Lee, 2014; Polinski *et al.*, 2018) and since expression levels of α-synuclein influence the propensity of aggregate formation (Hayashita-Kinoh *et al.*, 2006), we first needed to assess whether α-synuclein expression is comparable. No obvious differences in transgenic α-synuclein expression levels were found in cerebrospinal fluid (CSF) collected from aged A53T α-synuclein TG LAG3$^{-/-}$ (LAG3 KO) and A53T α-synuclein TG LAG3$^{+/+}$ (LAG3 WT) mice with SIMOA (**Fig. S5A**), an indication of similar human α-synuclein expression levels. We then bred A53T α-synuclein TG LAG3$^{-/-}$ (LAG3 KO) (n=7), A53T α-synuclein TG LAG3$^{+/-}$ (LAG3 hemizygous) (n=9), A53T α-synuclein TG LAG3$^{+/+}$ (LAG3 WT) (n=13), and LAG3$^{-/-}$ α-synuclein WT (n=9) mice, including both male and female mice. All A53T α-synuclein mice but not LAG3$^{-/-}$ α-synuclein WT mice developed severe α-synucleinopathy and had to be sacrificed, with a median survival of A53T α-synuclein mice of 263 days (regardless of LAG3 genotype; CI95%: 240-277; **Fig. 5A**). LAG3 knockout or hemizygosity had no influence on overall survival in this mouse line (A53T α-synuclein TG LAG3$^{-/-}$: 239 (CI95%: 218-278) days, A53T α-synuclein TG LAG3$^{+/-}$: 260 (CI95%: 231-286) days, A53T α-synuclein TG LAG3$^{+/+}$: 268 (CI95%: 244-295) days, LAG3$^{-/-}$ α-synuclein WT: no sign of disease after > 300 days), suggesting that the presence or absence of LAG3 does not influence survival of the A53T transgenic animals. Consistent with these results, LAG3 knockout did not yield

obvious changes in the mesencephalic distribution patterns of pS129 α-synuclein or thioflavin S-positive aggregates (**Fig. 5B**) in end-stage symptomatic mice. These results suggest that LAG3 plays little, if any, role in the propagation of α-synuclein pathology *in vivo*.

No difference in pS129 α-synuclein in hippocampal organotypic slice cultures of A53T LAG3$^{-/-}$, or LAG3$^{+/+}$ mice

We then reasoned that the effect of LAG3 in a murine model may be contingent on the utilization of α-synuclein PFFs as a seed. Alternatively, LAG3 may influence early α-synuclein lesion formation without modifying the survival or the end-stage pathology of mice. To this end, we cultured hippocampal slices of A53T α-synuclein TG or α-synuclein WT mice KO or WT for LAG3, respectively, and inoculated them with 5 µg α-synuclein PFFs. Organotypic slices were kept in culture for five weeks and the pS129-

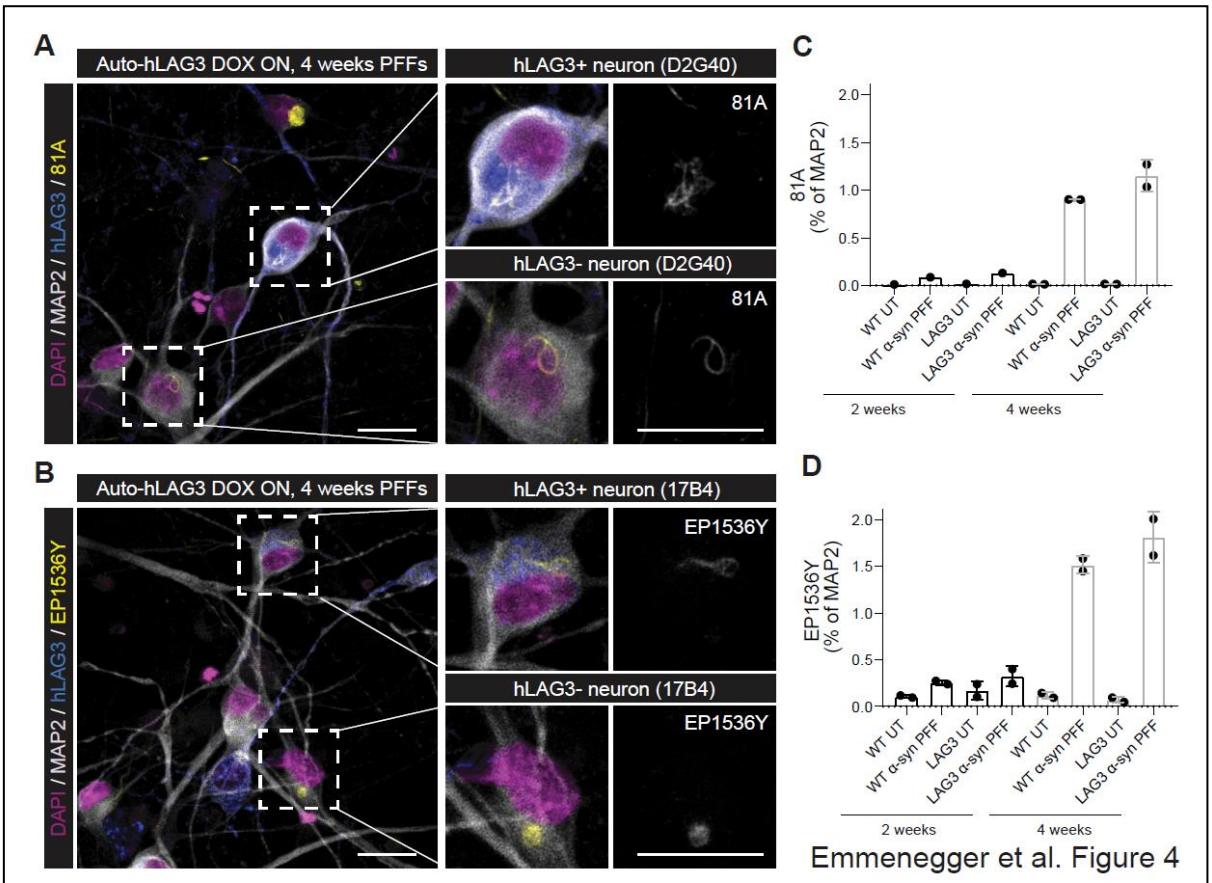

Fig. 4. **Propagation of α-synuclein PFFs in vitro is not dependent on LAG3 in human NSC-derived neural cultures**. Human neural cultures transduced by Auto-hLAG3 were treated by α-synuclein PFFs 4 days post LAG3 expression induction by DOX and kept in culture for 2 or 4 weeks (**A**-**D**). Both transgenic (hLAG3 D2G40-positive in **A** and 17B4-positive in **B**) and non-transduced, wild-type neurons (selected neurons in zoomed-in insets) propagated α-synuclein and developed characteristic pS129-positive (81A-positive in **A** and EP1536Y-positive in **B**) α-synuclein aggregates. Scale bars 25 µm. **C**. and **D**. Trained ilastik algorithms were used to segment pixels of 81A, EP1536Y and MAP2 stainings imaged by high-content wide-field microscope, which were used to quantify the signal of 81A-positive (**C**) and EP1536Y-positive (**D**) α-synuclein aggregates expressed as % of MAP2-positive area. Almost the entire wells (182 fields per well) were imaged for every condition and replicate and each datapoint in the plot represents the entire well. One-way ANOVA followed by Tukey's multiple comparison test demonstrated that neurons that did not express LAG3 (DOX OFF) showed no difference in α-synuclein propagation when compared to LAG3-expressing neurons (DOX ON) as demonstrated by two different pS129 α-synuclein antibodies (p=0.9998 for 81A at 2 weeks and p=0.2522 at 4 weeks; p=0.9986 for EP1536Y at 2 weeks and p=0.3042 at 4 weeks).

or thioflavin S-positive area was assessed (Barth *et al.*, 2021). Non-seeded organotypic slices did not show any sign of pS129 α-synuclein (**Fig. 5C**) or thioflavin S positivity (**Fig. 5D**), while seeded α-synuclein WT slices showed moderate pS129 α-synuclein- or thioflavin S-positive areas and A53T slices had more prominent pathology, as previously reported (Barth *et al.*, 2021). However, no significant difference was found between LAG3 KO and WT in slices derived from A53T transgenic or wildtype mice, indicat-

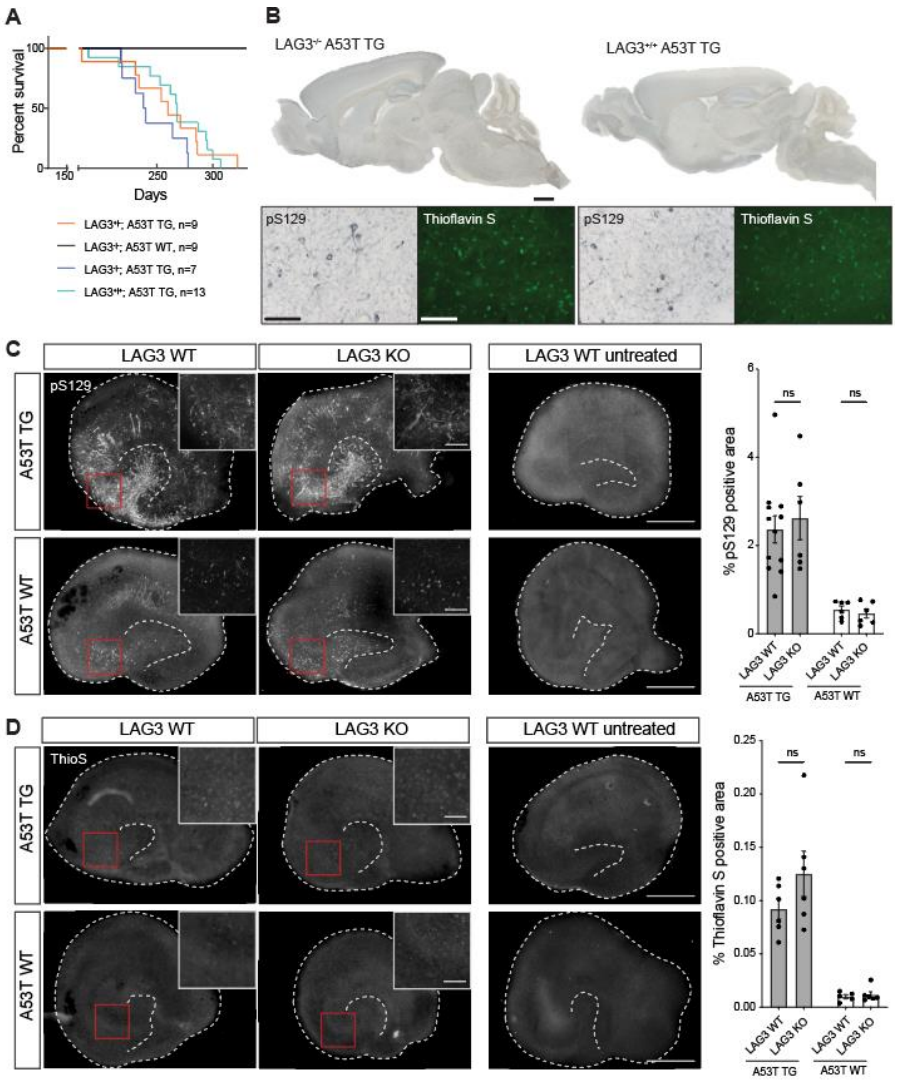

Fig. 5. **Survival in A53T α-synuclein mice and aggregation of α-synuclein in vivo and in hippocampal slice cultures is independent from LAG3 expression**. **A**. Survival curves of A53T α-synuclein TG mice, with LAG3 knockout, heterozygous LAG3 expression, or LAG3 WT. Median survival was shortest for α-synuclein TG LAG3$^{-/-}$ at 239 d, followed by α-synuclein TG LAG3$^{+/-}$ at 260 d and α-synuclein TG LAG3$^{+/+}$ at 268 d. Mice were euthanized and dissected in the late-stage symptomatic phase, which would inevitably result in death within a week. None of the control LAG3$^{-/-}$ α-synuclein WT mice died over the course of the experiment. **B**. Immunostaining for hyperphosphorylated α-synuclein aggregates (pS129) and aggregated protein (Thioflavin S) in sections of end-stage symptomatic mice; no obvious difference in terms of staining pattern or number of stained cells were apparent in midbrain or brain stem. **C**. Immunofluorescence staining and quantification of pS129-positive α-synuclein inclusions in hippocampal slice cultures (HSCs) at 5 weeks post-seeding with 350 µM PFF. Scale bars represent 500 µm (overview), and 100 µm (inserts). Shown is mean ± SEM and individual values are shown; n = 6 cultures per group; two-way-ANOVA revealed for LAG3 $F(1, 20) = 0.0294$; $p = 0.8656$; A53T $F(1, 20) = 36.42$, $p < 0.0001$; interaction $F(1, 20) = 0.0062$, $p = 0.9382$. Bonferroni's correction for multiple comparisons revealed $p = 0.9973$ for LAG3 WT vs. KO in A53T TG and $p > 0.9808$ for LAG3 WT vs. KO in A53T WT. **D**. Immunofluorescence staining and quantification of Thioflavin S-positive α-synuclein inclusions in HSCs at 5 weeks post-seeding. Scale bars represent 500 µm (overview), and 100 µm (inserts). Shown is mean ± SEM and individual values are shown; n = 5-6 cultures per group; two-way-ANOVA revealed for LAG3 $F(1, 19) = 1.972$, $p = 0.1763$; A53T $F(1, 19) = 62.49$, $p < 0.0001$; interaction $F(1, 19) = 1.586$, $p = 0.2231$. Bonferroni's correction for multiple comparisons revealed $p = 0.1373$ for LAG3 WT vs. KO in A53T TG and $p > 0.9999$ for LAG3 WT vs. KO in A53T WT.

Discussion

LAG3 was named a selective receptor for pathogenic α-synuclein assemblies using an exhaustive series of in vitro and in vivo experiments with a variety of genetic and pharmacological tools (Mao *et al.*, 2016). Yet there is little evidence for a role of LAG3 in human α-synucleinopathies (Liu *et al.*, 2018; Cui *et al.*, 2019; Guo *et al.*, 2019). This situation prompted us to revisit the interaction between LAG3 and α-synuclein conformers. When assessing cell lines, NSC-derived neural cultures, or organ homogenates for the presence of human or murine LAG3, we have strived to select antibodies appropriate to the species investigated and, whenever possible, have used multiple antibodies to increase the confidence in our results. Yet we were unable to detect LAG3 in any of the neuronal samples tested. Thus, we felt the need to investigate further using a broader array of techniques: Western Blotting, sandwich ELISA, immunofluorescence, RT-qPCR, snRNAseq, and scRNAseq. None of these methods were able to detect endogenous LAG3 expression in human neurons. The most parsimonious interpretation of these collective data is that human neurons do not express LAG3 at appreciable levels. One notable exception is our scRNAseq dataset of mouse ventral midbrain detecting low expression of LAG3 in microglia, in accordance with previous reports (Tasic *et al.*, 2016; Galatro *et al.*, 2017).

It is unclear whether the lack of detection of LAG3 in human microglia relates to a crucial species difference or to technical limitations of snRNAseq versus scRNAseq, which may be particularly important for microglia (Thrupp *et al.*, 2020). Either way, this data and other available datasets (Zhang *et al.*, 2014, 2016; Welch *et al.*, 2019; Agarwal *et al.*, 2020; Almanzar *et al.*, 2020) do not support expression of neuronal LAG3, at least using current technology for single cell analysis. Thereby, we question one of the foundations of the hypothesis proposed by (Mao *et al.*, 2016) and discussed elsewhere (Jucker and Heikenwalder, 2016; Wood, 2016; Wong and Krainc, 2017).

A possible confounder may be the cross-immunoreactivity of antibodies between murine and human LAG3, which appears to be rare. Within a collection of commercial anti-LAG3 antibodies, only one out of 8 anti-LAG3 antibodies reacted with both human as well as murine LAG3. Mao et al. immunoblotted the human HEK293FT and SH-SY5Y cell lines alongside mouse cortical cultures using an anti-LAG3 antibody (4-10-C9, MABF954) that appears to specifically recognize LAG3 of murine origin (see supplementary figure 5 in (Mao *et al.*, 2016)).

LAG3 could plausibly play a role in the pathogenesis of α-synucleinopathies, e.g. via complex formation with soluble LAG3 (Guo *et al.*, 2019) and subsequent endocytosis by hitherto unidentified neuronal receptors or via targeting immune checkpoints of T cells (Baruch *et al.*, 2016; Schwartz, 2017; Liu and Aguzzi, 2019) despite not being pulled down upon brief exposure of mouse primary neurons and astrocytes to α-synuclein fibrils (Shrivastava *et al.*, 2015). The interaction between LAG3 and fibrillary α-

synuclein is therefore of interest. α-synuclein fibrils, in contrast to Apoptosis-associated speck-like protein containing a CARD (ASC), are promiscuous, yet they bind some proteins much better than others. LAG3, the MTBD of human tau, and CD4 interacted more than PrP^C, APOE3 and TDP-43 in contrast with BSA and Ara h 2. However, the binding of α-synuclein fibrils to CD4 stands in direct opposition to data presented earlier (Mao *et al.*, 2016). FGL1, a recently reported interaction partner of LAG3 (Wang *et al.*, 2019), could be confirmed to bind LAG3 with microfluidic diffusional sizing (MDS), with an affinity of 232 ± 79 nM, slightly higher than a previous assessment with Octet bio-layer interferometry analysis suggested (Wang *et al.*, 2019). On the other hand, MDS failed to reproduce data obtained by ELISA, as no binding between LAG3 and α-synuclein fibrils occurred, nor with CD4 and α-synuclein fibrils. This could indicate that the nature of interaction differs between LAG3 and α-synuclein fibrils or FGL1. A possible explanation is that single α-synuclein fibrils bind to multiple LAG3 molecules through weak electrostatic interactions, resulting in cooperative unspecific interactions that can be captured with ELISA where proteins are immobilized, but not with MDS.

A pulldown experiment confirmed the weak interaction between LAG3 and α-synuclein fibrils. Due to the promiscuous binding of α-synuclein fibrils, their specificity to LAG3 seems questionable. Experiments performed by (Mao *et al.*, 2016) indicate that $LAG3^{-/-}$ reduces α-synuclein fibril binding in cortical neurons by maximally 10% (see figure 1D, in (Mao *et al.*, 2016)). In the original report, mean values in $LAG3^{-/-}$ primary cortical neurons differ only at high α-synuclein fibril-biotin concentrations and display a relatively high standard error (Mao *et al.*, 2016), suggesting that there was no biologically important difference. This is not surprising in view of LAG3 not being expressed in neuronal cultures, so its ablation should not have an effect. Our experiments in human neural cultures point in the same direction as we could not identify any significant difference in pS129-positive aggregates upon expression of LAG3, strongly suggesting that other neuronal factors, some of which we identified through a pulldown approach (Shrivastava *et al.*, 2015), mediate the uptake and transmission of α-synuclein fibrils.

Despite the negative findings above, LAG3 may exert a modulatory role in α-synucleinopathies through other mechanisms. We investigated whether LAG3 ablation changes the propensity of α-synuclein aggregation in vivo and, importantly, whether it affects the overall survival of α-synuclein-overexpressing mice. However, our study conducted in A53T human α-synuclein TG mice KO, hemizygous or WT for LAG3 showed that neither lifespan nor deposition of α-synuclein aggregates is significantly changed upon presence or absence of LAG3, leaving little hope that LAG3 would assume a role in α-synuclein-related pathologies. Experiments with hippocampal organotypic slice cultures inoculated with α-synuclein PFFs did not change this perception to the better, and do not seem to converge with the notion that LAG3 contributes to α-synucleinopathy in different A53T human α-synuclein mice (Gu *et al.*, 2021).

Parkinson's disease and other pathologies underlying the spread of α-synuclein aggregates are severe neurodegenerative diseases with momentous implications on the lives of patients and their families. More work is needed to understand how α-synuclein is transmitted from cell to cell, to identify selective receptors for propagating forms of α-synuclein and to subsequently enable a targeted treatment. Until then, potential targets need to be rigorously vetted, bearing in mind that attrition of futile approaches is crucial to avoiding high opportunity costs.

Methods and Materials

Antibodies used.

Name	Immunogen	Experiment
4-10-C9 mouse monoclonal antibody (MABF954, MerckMilli-pore)	Mouse LAG3	Mouse Western Blot, Mouse LAG3 sandwich ELISA, indirect ELISA
LS-B15026 rabbit polyclonal antibody (LSBio)	Mouse LAG3	Mouse Western Blot, indirect ELISA
rat mAb C9B7W	Mouse LAG3	Mouse LAG3 sandwich ELISA, indirect ELISA
LAG3 (D2G4O™) XP® Rabbit mAb #15372	Human LAG3	Human Western Blot, immunofluorescence, human LAG3 sandwich ELISA, indirect ELISA
Anti-LAG-3 antibody [17B4] (ab40466)	Human LAG3	Human Western Blot, immunofluorescence, indirect ELISA
Relatlimab anti-LAG3 antibody (BMS-986016)	Human LAG3	Human LAG3 sandwich ELISA, indirect ELISA
LAG525 (Novartis)	Human LAG3	Indirect ELISA
Mouse mAb human LAG-3 (Clone 874501)	Human LAG3	Indirect ELISA
Anti-Alpha-synuclein (phospho S129) antibody [P-syn/81A] (ab184674)	pS129 α-synuclein	Immunofluorescence
Recombinant Anti-Alpha-synuclein (phospho S129) antibody [EP1536Y] (ab51253)	pS129 α-synuclein	Immunofluorescence
Recombinant Anti-Alpha-synuclein antibody [MJFR1] (ab138501)	α-synuclein	ELISA with fibrils, immunofluorescence, Microfluidic diffusional sizing
Polyclonal rabbit anti-ASC antibody AL177 (AdipoGen, #AG-25B-0006)	ASC	ELISA with fibrils
Anti- Glial Fibrillary Acidic Protein (GFAP) (ab53554)	GFAP	Immunofluorescence analysis of mouse primary cultures
Anti-MAP2 antibody (ab5392)	MAP2	Immunofluorescence analysis of mouse primary cultures
Anti-Iba1 (WA3 019-19741)	Iba1	Immunofluorescence analysis of mouse primary cultures
HRP Donkey anti rat IgG (H+L), 712-035-153, Jackson		Secondary antibody, ELISA, Western Blot
HRP Goat anti Rabbit IgG (H+L), 111-035-045, Jackson		Secondary antibody, ELISA, Western Blot
HRP Goat anti-mouse IgG (H+L), 115-035-003, Jackson		Secondary antibody, ELISA, Western Blot
Peroxidase AffiniPure Goat Anti-Human IgG, Fcγ Fragment Specific, Jackson, 109-035-098		Secondary antibody, ELISA, Western Blot
Donkey anti rabbit AF568 (Invitrogen #A10042)		Secondary antibody, immunofluorescence
Donkey anti mouse AF488 (Invitrogen #A-21202)		Secondary antibody, immunofluorescence

Donkey anti chicken AF647 (Jackson Immuno Research #JAC703-606-155)	Secondary antibody, immunofluorescence

345

Antigens used

Name	Experiment
Human APOE3, PeproTech (#350-02)	ELISA with fibrils
Human ASC-C-his, produced by Matthias Geyer (Bonn)	ELISA with fibrils
Human LAG3$_{23-450}$, ACROBiosystems (#LA3-H5222)	ELISA with fibrils, antibody testing
Human LAG3$_{23-434}$, BonOpusBio (#CJ91)	MDS
Mouse LAG3$_{24-442}$, ACROBiosystems (#LA3-M52H5)	ELISA with fibrils, antibody testing
Natural Ara h 2 (NA-AH2-1), Light roasted peanut flour (Runner cultivar), Indoor Biotechnologies	ELISA with fibrils
Human recombinant PrP^{C}, produced in-house (Adriano Aguzzi)	ELISA with fibrils
Bovine serum albumin (BSA), Thermo Scientific	ELISA with fibrils, MDS
FGL1 Protein, Human, Recombinant, 13484-H08B, Sino Biological	MDS
Human α-synuclein, produced in-house (Kelvin Luk)	ELISA with fibrils
Human CD4, ACROBiosystems (#LE3-H5228)	ELISA with fibrils, MDS
MTBD tau, produced in-house (Adriano Aguzzi)	ELISA with fibrils

Mouse primary cultures

Mice housing were in accordance with the Swiss Animal Welfare Law and in compliance with the regulations of the Cantonal Veterinary Office, Zurich. For primary culture we used 8- to 9-week-old C57BL/6J mice. When needed, two pregnant females (E14) were delivered and housed in the animal facility of the University of Zurich. Primary neuronal cell cultures were prepared from brains of E16-17 mouse embryos. Briefly, hippocampus and cortex were isolated in PBS-Glucose (D-Glucose, 0.65 mg/ml). The tissue was treated with trypsin (0.5% w/v) in PBS-Glucose and dissociated in Neurobasal medium (NB) supplemented with glutamine (2 mM), 2% B27, 2% N2, 100U penicillin-streptomycin (P/S) and D-Glucose (0.65 mg/ml). In order to obtain a mixed culture, the medium was supplemented with 2.5% Horse Serum for the first 24h in vitro, while for neuronal-enriched culture, cells were treated with 5uM cytosine arabinoside (AraC) from DIV 1 to DIV 6. For biochemical experiments, cells were then plated onto poly-D-lysine coated 6-well- plate (TPP - 92006) at 8 x 10^5 cells/cm^2. For imaging, cells were plated onto poly-D-lysine coated chambered coverglass (NuncTM Lab- TekTM - 155411) at 2x10^5 cells/cm^2. For both types of culture, only one-half of the medium changed every 3-4 days. When lentiviral transduction was used to generate LAG3-expressing cultures, cells were transduced at DIV 6 and

fixed at DIV 13. Primary glia cell cultures were prepared from postnatal (P4-P6) pups. Briefly, hippocampus and cortex were isolated. The tissue was treated with trypsin (0.5% w/v) in HBSS-Glucose (D-Glucose, 0.65 mg/ml) and triturated with glass pipettes to dissociate tissue in DMEM/F12 (31330038) supplemented with glutamine (2 mM), 5% Horse Serum and 100U penicillin-streptomycin, 100uM non-essential amino acid and 2mM sodium pyruvate. For biochemical experiments, cells were plated 6-well- plate (TPP - 92006) at 8 x 10^5 cells/cm^2. For imaging, cells were plated onto chambered coverglass (NuncTM Lab- TekTM - 155411) at 2x10^5 cells/cm^2.

Synaptoneurosome preparations and region-specific dissections of murine brains

Synaptosome fractions were prepared following the protocol performed as described earlier (De Rossi *et al.*, 2020). Briefly, cortices, striata, and hippocampi were dissected from the brains of adult C57BL/6J mice and resuspended in cold buffer containing 0.32 M sucrose and 10 mM HEPES at pH 7.4 and centrifuged twice (at 770 x g) to remove nuclei and large debris, followed by centrifugation at 12'000 x g to obtain the synaptosome fraction. The synaptosomes were washed and pelleted in EDTA buffer to chelate calcium (4 mM HEPES, 1 mM EDTA, pH 7.4, 20 min at 12000 x g). The synaptosomes were resuspended in the lysis buffer for one hour on ice (20 mM HEPES, 0.15 mM NaCl, 1% Triton X-100, 1% deoxycholic acid, 1% SDS, pH 7.5) and stored at -80 °C. Region-specific dissections (cortex, hippocampus, olfactory bulb, corpus callosum, midbrain, striatum, hindbrain, cerebellum) were performed in the same mice and solubilized in 20 mM HEPES, 0.15 mM NaCl, 1% Triton X-100, 1% deoxycholic acid, 1% SDS, pH 7.5 and stored at -80 °C.

Isolation and activation of mouse T lymphocytes

T lymphocytes were isolated from the spleen of C57BL/6J mice using a negative selection isolation kit (EasySep™ Mouse T Cell Isolation Kit, StemCell Technologies). Cells were plated in a 48 wells plate (Corning) previously coated with anti-mouse CD3 (clone #17A2, PeproTech) and anti-mouse CD28 (clone #37.51, PeproTech) antibodies and incubated in IMEM medium supplemented with IL-2 at 37 °C. After 3 days, the activated T lymphocytes were collected and processed for either RNA extraction or Western Blotting. Expression of mLAG3 was checked by Western Blotting using mLAG3-transfected HEK cells as positive control.

Isolation and activation of human T lymphocytes

Fully anonymized residual full blood samples were collected at the Institute of Clinical Chemistry (USZ) using a workflow outlined previously (Emmenegger *et al.*, 2020) and peripheral blood mononuclear cells (PBMCs) were isolated using a Ficoll gradient. PBMCs were resuspended in RPMI medium supplemented with 10% FBS, 1x P/S, 1x non-essential amino acids (Gibco) and 1x sodium pyruvate (Gibco), to reach a concentration of 2 million cells per ml. 2 ml cell suspension/well was added into a 24-well

plate. 1 ml medium was removed every second day and 1 ml RPMI medium with supplements as listed above as well as with 100 international units IL-2 and 2 µg/ml phytohemagglutinin (PHA) was added. T cells were cultured between 7-9 days. Finally, the medium was removed, 100 µl lysis buffer (50 mM Tris, pH 8, 150 mM NaCl, 1% Triton, protease and phosphatase inhibitors) was added to each well and multiple wells were pooled. Following a centrifugation step (16'000g, 20 min, 4 °C), the supernatant was transferred to a clean tube and the protein concentration measured using the BCA assay.

Lentivirus preparation, transduction and SH-SY5Y cell line generation

Using NEBuilder HiFi DNA Assembly Cloning Kit (NEB #E5520), human or mouse LAG3 cDNA sequence (GeneCopoeia #EX-Z5714-M02 and #EX-Mm03576-M02) were inserted into an autoregulatory, all-in-one TetON cassette (AutoTetON; (Hruska-Plochan *et al.*, 2021)), which was previously inserted into a pLVX lentiviral transfer vector (Clontech # 632164), while deleting CMV-PGK-Puro, generating Auto-hLAG3 and Auto-mLAG3 lentiviral transfer vectors. These were then packaged into lentivirus via co-transfection with CMV-Gag-Pol (Harvard #dR8.91) and pVSV-G (Clontech, part of #631530) plasmids into production HEK293T cells adapted to grow in serum-free conditions (OHN media; (Hruska-Plochan *et al.*, 2021), which reduces the expression of the GOI from the transfer vector as well as it eliminates serum-carry over into the supernatant. Medium was changed the following morning and supernatants were then collected 48 hours post transfection (36 hours post media change), centrifuged at (500g, 10 min, 4 °C), filtered through Whatman 0.45 µm CA filter (GE #10462100) and concentrated using Lenti-X™ Concentrator (Takara #631232) according to producer datasheet (overnight incubation). The resulting lentiviral pellets were then resuspended in complete neuronal maturation media or OHN media to achieve 10x concentrated LV preparations, which were titrated using Lenti-X™ GoStix™ Plus (Takara #631280). Auto-hLAG3 had a GoStix Value (GV) of 6496 and Auto-mLAG3 had GV of 12839.

Transduction of human neural cultures

Differentiated human neural cultures (2 months old) were transduced with 250 µl of Auto-hLAG3 LV and 3 µg/ml of polybrene (Sigma-Aldrich #TR-1003-G) per well of a 6 well plate. Medium was exchanged completely the following day. hLAG3 expression was induced by 1 µg/ml of Doxycycline (DOX; Clontech #631311).

Transduction of SH-SY5Y cells to generate SH-10 line inducibly expressing hLAG3

SH-SY5Y human neuroblastoma cells (Sigma-Aldrich #94030304) at P11 were transduced in a 6 well plate using 300 µl of Auto-hLAG3 LV pre-incubated with 30 µl of Lenti-X™ Accelerator (Clontech #631256) for 30 min. The LV mixture was added onto the cells, evenly spread over the whole well and put into incubator onto a neodymium magnetic sheet (supermagnete #NMS-A4-STIC; adhesive force of 450 g/cm^2) for 10 min. Cells were then removed from the incubator, LV mixture was completely

removed, and fresh SH media added. Cells were kept until confluency and then sub-cultured with the neodymium magnet sheet kept under the plate. To remove remaining magnetic beads, cell pellet was resuspended in 1.5ml of SH media, pipetted into 1.5 ml Eppendorf tube and inserted into DynaMag™-2 Magnet (Invitrogen #12321D). Cell suspension was then removed from the tube leaving all magnetic beads in the tube. Quantification of P11+1 SH-10 cells showed that 76% of cells were expressing hLAG3 upon induction by 1 µg/ml of Doxycycline (DOX; Clontech #631311). This decreased to 59% in P11+2 and remained around 50% in the following passages. P11+3 was used for all experiments except for the CO-IP, where a later passage was used.

Maintenance of NSC-derived neural cultures

Human neural stem cells derived from iPSCs using manual selection based on colony morphology (Bohaciakova *et al.*, 2019) – iCoMoNSCs (Hruska-Plochan *et al.*, 2021), were differentiated for 2 months resulting in functional neural networks (Hruska-Plochan *et al.*, 2021). Shortly, iCoMoNSCs were plated onto Matrigel-coated 6-well plates and grown in NSC media until reaching confluency. Media was then changed to D3 differentiation media, which was replaced for maturation media at 4 weeks of differentiation. For imaging experiments, cultures were dissociated into single-cells suspension using Papain Dissociation System (Worthington #LK003150), passed through 70 µm cell strainer (Falcon #07-201-431), resuspended in maturation media and re-plated into 96 well imaging plate (Greiner Bio-One #655090) at 120'000 cells per well as counted by CASY Cell Counter (Innovatis AG).

scRNAseq in NSC-derived neural cultures – Sample preparation

Differentiated human neural cultures (3 months old) were dissociated into single-cells suspension using Papain Dissociation System (Worthington #LK003150), passed through 70µm and 40µm cell strainers (Falcon #07-201-431 and #07-201-430), and resuspended in HIBE++ media (Hibernate™-E Medium medium (Gibco #A1247601) supplemented with EDTA (1mM final; Invitrogen #AM9260G), HEPES (10mM final; Gibco #15630080), with 1X B27+ supplement (Gibco #17504-044), 1X N2 supplement (Gibco #17502-048); 1X GlutaMAX (Gibco #35050-061), BDNF (PeproTech #450-02), GDNF (Alomone labs #G-240), CNTF (Alomone labs #C-240), NT-3 (PeproTech #450-03) and IGF-1 (Stem Cell #78022) all at 20 ng/ml) to 1000 cells per µl using to CASY Cell Counter (Innovatis AG).

scRNAseq in NSC-derived neural cultures using 10X Genomics platform

The quality and concentration of the single cell preparations were evaluated using an haemocytometer in a Leica DM IL LED microscope and adjusted to 1,000 cells/µl. 10,000 cells per sample were loaded in to the 10X Chromium controller and library preparation was performed according to the manufacturer's indications (Chromium Next GEM Single Cell 3' Reagent Kits v3.1 protocol). The resulting libraries were sequenced in an Illumina NovaSeq sequencer according to 10X Genomics recommendations

(paired-end reads, R1=28, i7=8, R2=91) to a depth of around 50,000 reads per cell. The sequencing was performed at Functional Genomics Center Zurich (FGCZ).

scRNAseq data analysis in NSC-derived neural cultures - Cell clustering and differential expression on each sample

The fastq files were aligned to the Homo Sapiens reference sequence (build GRCh38.p13) taken from Ensembl. After the alignment, each observed barcode, UMI, gene combination was recorded as a UMI count matrix that was then filtered to remove low RNA content cells or empty droplets using the CellRanger software (v3.0.1). Starting from this matrix we used the R package Seurat (version 3.1.5) (Butler *et al.*, 2018) to perform the following downstream analyses per sample: genes and cells filtering, normalization, feature selection, scaling, dimensionality reduction, clustering and differential expression. We started by filtering out genes that didn't obtain at least 1 UMI count in at least 3 cells, and discarded cells for which fewer than 1500 genes or more than 8000 genes were detected and also those that had a mitochondrial genome transcript ratio greater than 0.12. After this, the data were normalized using a global-scaling normalization method that normalizes the feature expression measurements for each cell by the total expression, multiplies this by a scale factor (10,000 by default), and log-transforms the result. We next calculated a subset of 2000 features that exhibited high cell-to-cell variation in the dataset. Using as input these variable features, we performed PCA on the scaled data. Since Seurat clusters cells based on their PCA scores, we used a heuristic method called 'Elbow plot' to determine how many principal components (PCs) we needed to capture the majority of the signal. In this way, the cells were clustered with an unsupervised graph-based clustering approach using the first 30 first PCs and a resolution value of 0.5. Clusters were visualized using t-distributed Stochastic Neighbor Embedding of the principal components (spectral t-SNE) or Uniform Manifold Approximation and Projection for Dimension Reduction (UMAP) as implemented in Seurat. We found positive markers that defined clusters compared to all other cells via differential expression. The test we used was the Wilcoxon Rank Sum test which assesses separation between the expression distributions of different clusters. Genes with an average, at least 0.25-fold difference (log-scale) between the cells in the tested cluster and the rest of the cells, and an adjusted p-value < 0.01 were declared as significant. Cell-cycle phases were predicted using a function included in the scran R package (Lun, McCarthy and Marioni, 2016) that scores each cell based on expression of canonical marker genes for S and G2/M phases. To visually, qualitatively and quantitatively interrogate expression of particular genes in all cells amongst all clusters via t-SNE, UMAP, violin and distribution plots, we used a custom-built Shiny application.

Propagation experiment in NSC-derived neural cultures: PFF-induced synuclein aggregation and aggregates quantification

Human neural cultures were transduced as described above. 4 days later, neural cultures were sub-cultured into 96 well plates as described above. hLAG3 expression was then induced by addition of 1 µg/ml of Doxycycline (DOX; Clontech #631311) 3 weeks (4 week DOX on conditions) or 5 weeks (2 weeks DOX on conditions) later. 4 days post hLGA3 expression activation, 500 nM of human exogenous α-synuclein pre-formed fibrils (PFFs) produced from monomeric recombinant α-synuclein by Kelvin Luk lab as per (Volpicelli-Daley, Luk and Lee, 2014) were added to half of the wells (resulting in 8 conditions: 2 weeks $DOX^{+/-}$/ $PFFs^{+/-}$ (n = 4 wells per condition) and 4 weeks $DOX^{+/-}$/ $PFFs^{+/-}$ (n = 5 wells per condition)). 50 µl of fresh media was added 4 days and then again 6 days later and 50% of media was exchanged on day 8 of the treatment and then 3 times a week until the end of the experiment while refreshing the DOX at 1 µg/ml.

Propagation experiment in NSC-derived neural cultures: Fixation, immunofluorescence and imaging

Neural cultures were fixed with pre-warmed 16% methanol-free formaldehyde (Pierce #28908) pipetting it directly into the culture media, diluting it to 4% final, and incubated for 15 min at room temperature. Cells were then washed once with PBS (Gibco # 10010015) for 10 min, once with PBS with 0.2% Triton-X-100 (TX; Sigma #T9284) washing buffer (WB) for 10 min and then blocked with 10% normal donkey serum (Sigma-Aldrich #S30-M), 0.2% TX in PBS blocking buffer (BB) filtered via stericup (Millipore #S2GPU02RE) for 30 min at room temperature (RT). Primary antibodies were then diluted in BB blocking buffer (81A 1:500; D2G40 1:500; MAP2 Abcam #ab5392; EP1536Y 1:500; 17B4 1:500; MJFR-1 1:1000) and left incubated overnight (ON) at 4°C on an orbital shaker. Cells were then washed 3 x 15 min in WB at RT and secondaries were then diluted in BB blocking buffer (Donkey anti rabbit AF568 (Invitrogen #A10042) 1:750; Donkey anti mouse AF488 (Invitrogen #A-21202) 1:750; Donkey anti chicken AF647 (Jackson Immuno Research #JAC703-606-155) 1:500) and incubated for 1.5 hours at RT. Cells were then again washed 3 x 15 min in WB at RT with DAPI (Thermo Scientific #62248) diluted to 1 ug/ml in the final WT wash. Cells were finally washed 1 x 15 min in PBS at RT, and PBS was then added to the wells to store the stained cells at 4 °C. Human neural cultures were imaged using GE InCell Analyzer 2500 HS widefield microscope for quantification (40X air objective; 2D acquisition; 182 fields of view per well; 50µm separation to avoid counting cells twice) or with Leica SP8 Falcon inverted confocal for high power, high resolution microscopy (63X oil objective; 2096 x 2096 pixels at 0.059 µm/pixel, approx. 20-30 z-steps per stack at 0.3 µm). Laser and detector setting were kept same for each staining combination and all imaged conditions. Huygens professional (Scientific Volume Imaging, Hilversum, Netherlands) was then used to deconvolute the stacks and the deconvoluted images were further post-processed in fiji to produce a flattened 2D pictures (Z-projection) for data visualization.

Propagation experiment in NSC-derived neural cultures: Signal quantification

Trained ilastik (Berg *et al.*, 2019) algorithms were used to segment the pixels (positive vs background) of 81A, EP1536Y and MAP2 stainings. Segmented pictures (182 images per well, per channel) were then exported and the total signal quantified in fiji via batch processing using a custom macro. Sum of all positive pixels of all 182 fields of view per well for 81A and EP1536Y was then expressed as % of total MAP2 area occupied by 81A or EP1536Y signal. Statistical analysis was performed in Prism (GraphPad San Diego, CA, USA) and one-way ANOVA followed by Tukey's multiple comparison test was applied on the datasets.

Propagation experiment in NSC-derived neural cultures: PFFs preparation and treatment

PFFs were sonicated before their addition to the neural cultures as follows: stock PFFs at 5 mg/ml was diluted in PBS (Gibco # 10010015) inside of a standard 0.5ml Eppendorf tube to 0.1 mg/ml reaching 250 µl final volume. The diluted PFFs were then sonicated using ultrasonic processor (Qsonica #Q500A-110) equipped with a cup horn (Qsonica #431C2) allowing for indirect sonication via high intensity ultrasonic water bath using the following settings: Amplitude 40%, 30 cycles of 2 s on, 2 s off (resulting in total run time of 120 s; 60 s sonication, 60 s off). Ice-cold water was freshly poured into the cup immediately before the sonication. 210 µl of sonicated PFFs were further diluted in 2790 µl of pre-warmed complete maturation media (reaching 500 nM) and added to the neural cultures (250 µl per well; all spent media was removed before treatment).

snRNA sequencing in human frontal cortex

Single nuclei RNA sequencing (snRNAseq) analysis of human frontal cortex was completed as previously described (Saez-Atienzar *et al.*, 2021). In brief, frozen frontal cortex tissue samples from 16 donors in the North American Brain Expression Consortium study series (dbGaP Study Accession: phs001300.v1.p1, (Myers *et al.*, 2007)) were obtained from the University of Maryland Brain and Tissue Bank through the NIH NeuroBioBank. Nuclei were isolated from 21 total samples from the 16 donors by ultracentrifugation through a sucrose gradient, and the Chromium Single Cell Gene Expression Solution v3 (10x Genomics) was used to construct snRNAseq libraries. Libraries were pooled and sequenced using the Illumina NextSeq 550 System. The resulting FASTQ files were aligned and counted using Cell Ranger v3 (10x Genomics). The 21 datasets were integrated and clustering analysis was performed using Seurat v3.1 (Stuart *et al.*, 2019) in R. Cell clusters comprised of a total of 161,225 nuclei were manually assigned cell type identities based on differential expression of known cell type marker genes. The cell type abbreviations are as follows: "EC" = Endothelial Cell; "AST" = Astrocyte; "MGL" = Microglia; "OPC" = Oligodendrocyte Precursor Cell; "ODC" = Oligodendrocyte; "InN" = Inhibitory Neuron; "ExN" = Excitatory Neuron.

scRNA sequencing in mouse mesencephalon and striatum

Single cell suspensions were generated from the midbrain and striatum of 1 year old animals. All the animals have received a single intra-striatal injection with either lipopolysaccharide (LPS) or phosphate buffered saline (PBS) and were sacrificed 48 hours after surgery as described previously (Russo *et al.*, 2019). Brain areas were dissociated using Adult Brain Dissociation Kit (Miltenyi Biotec #130-107-677) following by myelin removal with 20 µl myelin removal beads (Miltenyi Biotec #130-096-733). Cell concentration and viability of the single cell solutions were determined on LunaFL cell counter (Logos Biosystems) and adjusted to 1'000 cells per µl. Preparations had more than 85% viability and were kept on ice prior to single cell encapsulation and library preparation. For encapsulation, 8'500 cells per sample were loaded into a Single-Cell 3' Chip of the 10X Chromium controller and libraries were generated using 10xGenomics (Chromium Next GEM Single Cell 3' Reagent Kits v3.1 protocol). The resulting libraries were examined by Agilent Bioanalyzer 2100 using a High Sensitivity DNA chip (Agilent). Libraries were sequenced at NIH Intramural Sequencing Center (NISC, Bethesda, USA) on an Illumina NovaSeq600 sequencer, using S4 flow cell format according to 10X Genomics recommendations (2x150bp, paired-end reads, Read1=28, i7 Index=8, Read2=91) with an estimated read depth of 100'000 reads per cell.

Sequencing data was analyzed using the Cell Ranger Pipeline (version v3.1.0) to perform quality control, sample demultiplexing, barcode processing, alignment and single-cell 3' gene counting. Genome Reference Consortium Mouse Build 38 (GRCm38-mm10) Mus musculus reference transcriptome was used for alignment. Single cell data from PBS or LPS treated animals were combined into a single Seurat object and filtered for genes detected in more than three cells and for cells that had more than 500 genes (features). These datasets were normalized using SCTransform v0.2.1 and integrated by pairwise comparison of anchor gene expression within the Seurat package v3.1 in R (Butler *et al.*, 2018). Shared nearest neighbor–based clustering was used to identify distinct cell clusters, which were then manually assigned cell type identities based on differential expression of known cell type marker genes.

Western Blotting

Whole mouse brains were homogenised in RIPA buffer, whereas mouse primary cortical cultures and activated T lymphocytes were lysed in lysis buffer (50 mM Tris, 150 mM NaCl, 1% Triton X-100) containing protease and phosphatase inhibitors (Roche, New York, NY, USA). Total protein contents were quantified using the BCA assay (Pierce). For Western Blotting, total proteins were separated on SDS-polyacrylamide gels (4-12%, Invitrogen) and transferred onto PVDF membranes. Membranes were blocked in 5% SureBlock (LubioScience) for 1 hour at RT and incubated overnight at 4°C with anti-LAG3 mouse monoclonal antibody 4-10-C9 (1:1'000). Membranes were washed three times with PBS-Tween

and incubated with goat-anti mouse IgG conjugated with horseradish peroxidase (1:10'000). The acquisition was performed using ECL Crescendo substrate (Merck Millipore) and imaged with Fusion Solo S (Vilber). After the acquisition, the membranes were incubated for 30 min at RT with anti- β-actin (1:10'000, A3854 Sigma-Aldrich), which is used as a normalizer.

For IP enrichment, 500 µg of total proteins of mouse brain homogenates and primary cultures and 10 µg of total proteins of activated T lymphocytes were incubated overnight with 50 µL of Dynabeads™ (ThermoFisher) previously conjugated with 4-10-C9 antibody. Beads were washed three times with PBS, resuspended in Laemli buffer and detached by boiling for 5 min at 95°C. The supernatants were loaded onto SDS-polyacrilamide gels and processed as described above. Target antigens were detected using an anti-LAG3 rabbit polyclonal antibody (1:1'000, B15026) and goat-anti rabbit IgG conjugated to horseradish peroxidase (HRP) (1:1'000).

Mouse LAG3 Sandwich ELISA

High-binding 384-well SpectraPlates (Perkin Elmer) were coated with mouse mAb 4-10-C9 at a concentration of 1 µg/mL in sterile PBS and at a volume of 20 µl/well. The plates were incubated for 1 hr at 37 °C and washed 3x with 1x PBS 0.1% Tween-20. Plates were then blocked with 5% milk in 1x PBS 0.1% Tween-20 (40 µl/well) and incubated for 1 hr at RT. The blocking buffer was subsequently removed. The cell lysates/organ homogenates were added at a total protein concentration of 1000 µg/ml (or, if indicated, at 500 µg/ml due to insufficient sample concentration), 20 µl/well, in quadruplicates and mouse recombinant $LAG3_{24-442}$ was added at 5 µg/ml at highest concentration, 40 µl/well into the first well of the dilution series, and a 15-fold 1:2 serial dilution of the recombinant proteins was performed (end volume for each well: 20 µl). The buffer used for sample dilution: 1% milk in 1x PBS 0.1% Tween-20. The plates were incubated for 1 hr at RT, followed by a 3x wash with 1x PBS 0.1% Tween-20. To detect the presence of LAG3, we used rat mAb C9B7W (for mouse LAG3), at 1 µg/ml and at 20 µl/well. The plates were incubated for 1 hr at RT, followed by a 5x wash with 1x PBS 0.1% Tween-20. To detect the presence of the detection antibody, we used HRP-anti-rat IgG (1:2'000, for mouse LAG3, HRP Donkey anti rat IgG (H+L), 712-035-153, Jackson), at volume of 20 µl/well. The plates were then incubated for 1 hr at RT and washed 3x with 1x PBS 0.1% Tween-20. TMB was dispensed at a volume of 20 µl/well, followed by a 5 min incubation, and the stop solution (0.5 M H_2SO_4) was added at a volume of 20 µl/well. The absorbance at 450 nm was read on the EnVision (Perkin Elmer) reader. Finally, the measured optical densities were interpolated (independently for all replicates) using the mouse recombinant LAG3 standards (values that are in the linear range) and LAG3 expression per µg total protein was depicted for all samples.

RNA extraction and RT-qPCR

Mouse primary cultures were collected and lysed in lysis buffer and Trizol LS Reagent in a ratio 1:3. Samples were supplemented with 0.2 mL of chloroform per 1 ml of Trizol and centrifugated. The aqueous phase was collected and the RNA was precipitated with subsequent addition of isopropanol and ice cold 75% ethanol. Pellets were resuspended in ultrapure, RNAse-free water and quantified at the Nanodrop. Genomic DNA elimination and reverse transcription were performed using QuantiTect Reverse Transcription Kit (Qiagen) according to manufacturer's instructions.

To generate a standard curve for transcript quantification, a commercial plasmid encoding full-length mouse LAG3 CDS (GeneCopoeia, Mm0357-02) was used as standard. The number of DNA molecules in 1 µl was calculated using the following formula:

$$\frac{copy\ number}{\mu l} = \frac{ng}{\mu l} * \frac{6.022 * 10^{23}}{(number\ bp\ vector + LAG3\ amplicon\ bp) * 10^9 * 650}$$

Serial dilutions of the standard containing known numbers of molecules and 25 ng of total cDNA of the samples were amplified in RT-qPCR using mouse LAG3-specific primers (Liu *et al.*, 2018). The number of transcripts per ng of RNA were calculated by interpolating the threshold cycle values of the samples into the standard curve and then dividing by the ng of RNA used in the RT-qPCR reaction.

ELISA with fibrils

High-binding 384-well SpectraPlates (Perkin Elmer) were coated with proteins of interest at a concentration of 1 µg/ml in sterile PBS and at a volume of 20 µl/well. The plates were incubated for 1 hr at 37 °C and washed 3x with 1x PBS 0.1% Tween-20. Plates were then blocked with 5% SureBlock (Lubio) in 1x PBS 0.1% Tween-20 (40 µl/well) and incubated for 1 hr at RT. The blocking buffer was subsequently removed. Monomer equivalents of fibrils (α-synuclein or ASC) were added at a concentration of 0.125 µM, 20 µl/well and a 13-fold 1:2 serial dilution was performed (end volume for each well: 20 µl). The buffer used for sample dilution: 1% SureBlock in 1x PBS 0.1% Tween-20. The plates were incubated overnight at 4 °C, followed by a 5x wash with 1x PBS 0.1% Tween-20. In a control experiment, monomer equivalents of fibrils (α-synuclein or ASC) were coated onto high-binding 384-well SpectraPlates (Perkin Elmer) as serial dilutions (13-fold 1:2 serial dilution), starting at a concentration of 0.125 µM, in sterile PBS and at a volume of 20 µl/well, incubated for 1 hr at 37 °C, washed 3x with 1x PBS 0.1% Tween-20, and blocked with SureBlock. Next, antibodies directed against the fibrils or monomeric proteins were added at 1 µg/ml and at 20 µl/well, in sample buffer. The plates were incubated for 1 hr at RT, followed by a 3x wash with 1x PBS 0.1% Tween-20. To detect the presence of the detection antibody, we used HRP-anti-rabbit IgG (1:2'000, HRP Goat anti Rabbit IgG (H+L), 111-035-045, Jackson), at volume of 20 µl/well. The plates were then incubated for 1 hr at RT and washed 3x with 1x PBS 0.1%

Tween-20. TMB was dispensed at a volume of 20 µl/well, followed by a 5 min incubation, and the stop solution (0.5 M H_2SO_4) was added at a volume of 20 µl/well. The absorbance at 450 nm was read on the EnVision (Perkin Elmer) reader and the respective curves were plotted in GraphPad Prism.

Microfluidics Diffusional Sizing

Microfluidic diffusional sizing (MDS) measurements were performed as reported previously (Arosio *et al.*, 2016; Wright *et al.*, 2018; Schneider *et al.*, 2020). Briefly, microfluidic devices were fabricated in polydimethyl siloxane (PDMS) applying standard soft-lithography methods and subsequently bonded onto a glass microscopy slide after activation with oxygen plasma. Samples and buffer were loaded onto the chip from sample reservoirs connected to the inlets and the flow rate controlled by applying a negative pressure at the outlet using a glass syringe (Hamilton, Bonaduz, Switzerland) and a syringe pump (neMESYS, Cetoni GmbH, Korbussen, Germany). Imaging was performed using a custom-built inverted epifluorescence microscope supplied with a charge-coupled-device camera (Prime 95B, Photometrics, Tucson, AZ, USA) and brightfield LED light sources (Thorlabs, Newton, NJ, USA). Lateral diffusion profiles were recorded at 4 different positions along the microfluidic channels. Varying fractions of unlabeled ligands were added to a solution containing labelled receptors of concentrations varying between 10 nM and 10 µM, and PBS (containing 0.01 % Tween 20, SA) was added to give a constant volume of 30 µL. The samples were incubated at room temperature for 60 minutes and the size of the formed immunocomplex was determined through measuring the hydrodynamic radius, R_h, with microfluidic diffusional sizing, as described above. Dissociation constants (K_D) were determined using the Langmuir binding isotherm, as previously reported (Schneider *et al.*, 2020),

$$\mathrm{R_h} = \left(\frac{[\mathrm{L}]_{tot} + \alpha[X]_0 + K_D - \sqrt{(\alpha[L]_{tot} + [X]_0 + K_D)^2 - 4\alpha[L]_{tot}[X]_0}}{2} \right) \frac{\Delta R}{\alpha[X]_0} + R_0$$

with $[L]_{tot}$ the concentration of ligand added, $[X]_0$ the concentration of labelled protein, K_D the dissociation constant, α the stoichiometric binding ratio, ΔR the difference in radius between fully bound and fully unbound, and R_0 the radius of fully unbound labelled protein.

Co-immunoprecipitation

SH-SY5Y cells expressing human LAG3 under the control of a doxycycline-inducible promoter were plated in 6-well plates and treated with doxycycline (1 µg/mL) for 72 hours to induce the expression of LAG3. Monomeric and fibrillar α-synuclein (1 µM) and PBS (negative control) were added to the culture medium and incubated for 3 hours at 37 °C. Cells were lysed in lysis buffer (50 mM Tris, pH 8,

150 mM NaCl, 1% Triton, protease and phosphatase inhibitors) and 500 µg of total proteins were further processed. 30 µL were collected from each sample and used as control inputs. Samples were pre-incubated with Dynabeads Protein G to eliminate any possible material that could bind unspecifically to the beads. Subsequently, samples were incubated with Dynabeads functionalized with either anti-α-synuclein or anti-LAG3 antibodies and left overnight on a rotor wheel at 4°C. The day after, beads were collected, resuspended in Laemli buffer and boiled for 5 minutes to detach the precipitated fractions. Supernatants were then loaded onto an SDS-PAGE and processed as described above.

Immunofluorescence

Primary cultures were fixed at DIV 12-14 with 4% PFA supplemented with 4% sucrose, followed by incubation in 10% donkey serum + 0.2% Triton-X100 for 1 hour at room temperature. For immunostaining, antibodies were diluted in blocking buffer (anti-MAP2 1:1'000; anti-GFAP 1:1'000; anti-LAG3 4-10-C9 1:1'000; anti-Iba1 1:1'000) and incubated overnight at 4°C. Samples were then washed 3 times with PBS and incubated with fluorescently-conjugated secondary antibodies (1:400) and DAPI (1:10'000).

Humanized mice

A53T-α-synuclein (Thy1-hA53T-αS) (Van Der Putten *et al.*, 2000) and LAG3 KO (B6.129S2-*LAG-3*^{tm1Doi}/J) (Miyazaki *et al.*, 1996) animals were bred and kept under specific pathogen-free conditions at the Hertie Institute for Clinical Brain Research in Tübingen, Germany. For estimation of survival rates, genders were balanced within the groups, whereas only female mice were used for immunological and Thioflavin-S staining. LAG3 KO mice were initially purchased from Jackson Laboratories (Bar Harbor, ME, USA) and crossed to our internal strains to generate the various genotypes used in this study. The experimental procedures were carried out in accordance with the veterinary office regulations of Baden-Wuerttemberg (Germany) and approved by the local Animal Care and Use Committees.

Preparation and treatment of hippocampal slice cultures

HSCs were prepared from pups at postnatal day 4-6 (P4-6) according to previously published protocols (Novotny *et al.*, 2016). After decapitation, the brains of the pups were aseptically removed, the hippocampi were dissected and cut perpendicular to the longitudinal axis into 350 µm sections with a tissue chopper. Carefully selected intact hippocampal sections were transferred into petri dishes containing ice-cold buffer solution (minimum essential medium (MEM) supplemented with 2 mM GlutaMAX™ at pH 7.3). Three sections were placed onto a humidified porous membrane in a well of a 6-well plate with 1.2 ml culture medium (20 % heat-inactivated horse serum in 1x MEM complemented with GlutaMax™ (1 mM), ascorbic acid (0.00125 %), insulin (1 µg/ml), $CaCl_2$ (1 mM), $MgSO_4$ (2 mM) and D-glucose (13 mM) adjusted to pH 7.3). HSCs were kept at 37°C in humidified CO_2-enriched atmosphere.

The culture medium was changed three times per week. HSCs were kept for 10 days without any experimental treatment. At day 10, 1 µL of PFF (5 µg/µL) was pipetted on top of each culture.

α-synuclein PFF preparation (Melki protocol)

Expression in *E. coli*, purification and quality control of human recombinant monomeric wt α-synuclein was done as previously described (Bousset *et al.*, 2013). For fibril formation, soluble wt α-synuclein was incubated in Tris-HCl buffer (50 mM Tris-HCl, pH 7.5, 150 mM KCl) at 37 °C under continuous shaking for 5 days and formation of fibrils was assessed with Thioflavin T. The fibrils were quality checked by transmission electron microscopy after negative staining before and after fragmentation. Their limited proteolytic pattern was also assessed (Bousset *et al.*, 2013). The average size of the fibrils after fragmentation 47 ± 5 nm was derived from length distribution measurements and their average molecular weight (16'200 Da) was derived from analytical ultracentrifugation sedimentation velocity measurements. The fibrils (350 µM) were aliquoted (6 µl per tube), flash frozen in liquid nitrogen and stored at -80 °C.

α-synuclein PFF preparation

Expression in *E. coli*, purification and quality control of human recombinant monomeric wt α-synuclein and assembly into PFFs was done as previously described (Luk *et al.*, 2009; Volpicelli-Daley, Luk and Lee, 2014). In brief, α-synuclein was expressed in *E. coli* and purified to reach a final concentration of monomeric α-synuclein of around 30 mg/ml. Monomeric α-synuclein in 1.5 ml microcentrifuge tubes at a volume of 500 ul and a final concentration of 5 mg/ml was assembled into α-synuclein PFFs by shaking for 7 days at 1000 RPM in a thermomixer at 37 °C. The quality of the fibrils was assessed as detailed earlier (Volpicelli-Daley, Luk and Lee, 2014).

Analysis of human α-synuclein expression in CSF of A53T LAG3$^{-/-}$ and LAG3$^{+/+}$ animals using SIMOA

Samples of the Cerebrospinal Fluid (CSF) were collected in a standardized manner adapted from the methodology of the Alzheimer's Association external quality control program used for human CSF (Mattsson *et al.*, 2011) as described previously (Schelle *et al.*, 2017). Sampling was performed under a dissecting microscope. Mice were deeply anesthetized with a mixture of ketamine (100 mg/kg) and xylazine (10 mg/kg) and placed on a heat pad to maintain a constant body temperature during the whole procedure. After incision of the overlying skin and retraction of the posterior neck muscles, the dura mater covering the cisterna magna was carefully cleaned with cotton swabs, PBS and ethanol. In case of microbleeds in the surrounding tissue, hemostyptic gauze (Tabotamp, Ethicon) was used to keep the dura mater spared from any blood contamination. Finally, the dura was punctured with a 30G needle (BD Biosciences) and CSF was collected with a 20 µl gel loader tip (Eppendorf, shortened), transferred into 0.5 ml polypropylene tubes (Eppendorf) and placed on ice. Typically, a total volume of 15–

25 µl was collected per mouse. The samples were centrifuged for 10 min at 2000xg, visually inspected for any pellet revealing blood contamination, aliquoted (5 µl) and stored at –80 °C until further usage. Samples with suspected blood or cell contamination were not used for any further experiments. CSF α-synuclein concentrations were measured by Single Molecule Array (SIMOA) technology using the SIMOA Human Alpha-Synuclein Discovery Kit according to the manufacturer's instructions (Quanterix, Billerica, MA, USA). Mouse CSF samples were diluted 1:300 with Alpha-Synuclein Sample Diluent before the measurement and analysed on a SIMOA HD-1 Analyzer in duplicates.

Histology and Immunohistochemistry

Brains were cut in 25 µm-thick sagittal sections on a freeze-sliding microtome (Leica SM 2000R) and subsequently emerged in cryoprotectant (35% ethylene glycol, 25% glycerol in PBS) and stored on -20 °C. Hippocampal cultures were fixed after 5 weeks of cultivation period with 4 % paraformaldehyde (PFA) in 0.1 M phosphate buffer (PB), pH 7.4 for 2 h. Cultures were rinsed 3 times with 0.1 M PBS for 10 min. The Millipore membrane with the fixed cultures was cut out and mounted onto a planar agar block. The cultures were sliced into 50 µm sections with a vibratome. Antigen retrieval was enhanced by heating the sections in 10 mM citrate buffer (1.8 mM citric acid, 8.2 mM trisodium citrate [pH 6.0]; 90 °C; 35 min). For detection of α-synuclein phosphorylated at ser-129, we used a rabbit monoclonal pS129 antibody (Abcam, EP1536Y, 1:1'000) and followed the standard protocols provided with the Vectastain Elite ABC Kit and the SG blue kit (Vector Laboratories, USA) (brain sections) or used an Alexa-fluorophore-conjugated secondary antibody (goat-anti-rabbit Alexa-568; Thermo Fisher, A11011) in a concentration of 1:250 (slice cultures). For Thioflavin S staining, sections were incubated for 5 min with freshly prepared filtered Thioflavin S solution (3% w/v Thioflavin S in milliQ H_2O) and washed 2x in 70% EtOH and 3x in milliQ H_2O for 10 min each.

Quantification of immunohistochemical stainings in slice cultures

For the quantification of the pS129-positive inclusions in HSCs, whole culture mosaic images were acquired on an Axioplan2 imaging microscope (Plan Neofluar 10x/0.50 objective lens; Zeiss). Images were blinded, colour channels were split, background was subtracted (rolling ball radius 50 pixels), and the intensity threshold was manually adjusted. On each mosaic, the percentage of pS129 positive signal over the whole culture was calculated. Statistical analysis was done with GraphPad Prism (v.9), using unpaired two-tailed t test.

References

Agarwal, D., Sandor, C., Volpato, V., Caffrey, T. M., Monzón-Sandoval, J., Bowden, R., Alegre-Abarrategui, J., Wade-Martins, R. and Webber, C. (2020) 'A single-cell atlas of the human substantia nigra reveals cell-specific pathways associated with neurological disorders', *Nature Communications*, 11(1), pp. 1–11. doi: 10.1038/s41467-020-17876-0.

Aguzzi, A. (2009) 'Cell biology: Beyond the prion principle', *Nature*. Nature Publishing Group, pp. 924–925. doi: 10.1038/459924a.

Aguzzi, A. and Lakkaraju, A. K. K. (2016) 'Cell Biology of Prions and Prionoids: A Status Report', *Trends in Cell Biology*. Elsevier Ltd, pp. 40–51. doi: 10.1016/j.tcb.2015.08.007.

Almanzar, N., Antony, J., Baghel, A. S., Bakerman, I., Bansal, I., Barres, B. A., Beachy, P. A., Berdnik, D., Bilen, B., *et al.* (2020) 'A single-cell transcriptomic atlas characterizes ageing tissues in the mouse', *Nature*, 583(7817), pp. 590–595. doi: 10.1038/s41586-020-2496-1.

Andrews, L. P., Marciscano, A. E., Drake, C. G. and Vignali, D. A. A. (2017) 'LAG3 (CD223) as a cancer immunotherapy target', *Immunological Reviews*. Blackwell Publishing Ltd, pp. 80–96. doi: 10.1111/imr.12519.

Arosio, P., Müller, T., Rajah, L., Yates, E. V., Aprile, F. A., Zhang, Y., Cohen, S. I. A., White, D. A., Herling, T. W., *et al.* (2016) 'Microfluidic diffusion analysis of the sizes and interactions of proteins under native solution conditions', *ACS Nano*, 10(1), pp. 333–341. doi: 10.1021/acsnano.5b04713.

Ascierto, P. A., Melero, I., Bhatia, S., Bono, P., Sanborn, R. E., Lipson, E. J., Callahan, M. K., Gajewski, T., Gomez-Roca, C. A., *et al.* (2017) 'Initial efficacy of anti-lymphocyte activation gene-3 (anti–LAG-3; BMS-986016) in combination with nivolumab (nivo) in pts with melanoma (MEL) previously treated with anti–PD-1/PD-L1 therapy.', *Journal of Clinical Oncology*, 35(15_suppl), p. 9520. doi: 10.1200/JCO.2017.35.15_suppl.9520.

Bae, J., Lee, S. J., Park, C.-G., Lee, Y. S. and Chun, T. (2014) 'Trafficking of LAG-3 to the Surface on Activated T Cells via Its Cytoplasmic Domain and Protein Kinase C Signaling', *The Journal of Immunology*, 193(6), pp. 3101–3112. doi: 10.4049/jimmunol.1401025.

Barth, M., Bacioglu, M., Schwarz, N., Novotny, R., Brandes, J., Welzer, M., Mazzitelli, S., Häsler, L. M., Schweighauser, M., *et al.* (2021) 'Microglial inclusions and neurofilament light chain release follow neuronal α-synuclein lesions in long-term brain slice cultures', *In submission*.

Baruch, K., Deczkowska, A., Rosenzweig, N., Tsitsou-Kampeli, A., Sharif, A. M., Matcovitch-Natan, O., Kertser, A., David, E., Amit, I., *et al.* (2016) 'PD-1 immune checkpoint blockade reduces pathology and

improves memory in mouse models of Alzheimer's disease', *Nature Medicine*, 22(2), pp. 135–137. doi: 10.1038/nm.4022.

Beitz, J. M. (2014) 'Parkinson's disease: A review', *Frontiers in Bioscience - Scholar*. Frontiers in Bioscience, pp. 65–74. doi: 10.2741/s415.

Berg, S., Kutra, D., Kroeger, T., Straehle, C. N., Kausler, B. X., Haubold, C., Schiegg, M., Ales, J., Beier, T., *et al.* (2019) 'ilastik: interactive machine learning for (bio)image analysis', *Nature Methods*, 16(12), pp. 1226–1232. doi: 10.1038/s41592-019-0582-9.

Bohaciakova, D., Hruska-Plochan, M., Tsunemoto, R., Gifford, W. D., Driscoll, S. P., Glenn, T. D., Wu, S., Marsala, S., Navarro, M., *et al.* (2019) 'A scalable solution for isolating human multipotent clinical-grade neural stem cells from ES precursors', *Stem Cell Research & Therapy*, 10(1), p. 83. doi: 10.1186/s13287-019-1163-7.

Bousset, L., Pieri, L., Ruiz-Arlandis, G., Gath, J., Jensen, P. H., Habenstein, B., Madiona, K., Olieric, V., Böckmann, A., *et al.* (2013) 'Structural and functional characterization of two alpha-synuclein strains', *Nature Communications*, 4(1), p. 2575. doi: 10.1038/ncomms3575.

Butler, A., Hoffman, P., Smibert, P., Papalexi, E. and Satija, R. (2018) 'Integrating single-cell transcriptomic data across different conditions, technologies, and species', *Nature Biotechnology*, 36(5), pp. 411–420. doi: 10.1038/nbt.4096.

Camisaschi, C., Casati, C., Rini, F., Perego, M., De Filippo, A., Triebel, F., Parmiani, G., Belli, F., Rivoltini, L., *et al.* (2010) 'LAG-3 expression defines a subset of CD4(+)CD25(high)Foxp3(+) regulatory T cells that are expanded at tumor sites', *J Immunol*, 184(11), pp. 6545–6551. doi: 10.4049/jimmunol.0903879.

Corbillé, A. G., Letournel, F., Kordower, J. H., Lee, J., Shanes, E., Neunlist, M., Munoz, D. G., Derkinderen, P. and Beach, T. G. (2016) 'Evaluation of alpha-synuclein immunohistochemical methods for the detection of Lewy-type synucleinopathy in gastrointestinal biopsies', *Acta neuropathologica communications*, 4, p. 35. doi: 10.1186/s40478-016-0305-8.

Cui, S. shuang, Du, J. J., Liu, S. H., Meng, J., Lin, Y. Q., Li, G., He, Y. X., Zhang, P. C., Chen, S., *et al.* (2019) 'Serum soluble lymphocyte activation gene-3 as a diagnostic biomarker in Parkinson's disease: A pilot multicenter study', *Movement Disorders*, 34(1), pp. 138–141. doi: 10.1002/mds.27569.

Deweerdt, S. (2016) 'Parkinson's disease: 4 big questions', *Nature*. Nature Publishing Group, p. S17. doi: 10.1038/538S17a.

Dickson, D. W. (2012) 'Parkinson's disease and parkinsonism: Neuropathology', *Cold Spring Harbor Perspectives in Medicine*, 2(8). doi: 10.1101/cshperspect.a009258.

Emmenegger, M., De Cecco, E., Lamparter, D., Jacquat, R. P. B., Ebner, D., Schneider, M. M., Condado Morales, I., Schneider, D., Dogancay, B., *et al.* (2020) 'Early peak and rapid decline of SARS-CoV-2 seroprevalence in a Swiss metropolitan region', *medRxiv*.

Galatro, T. F., Holtman, I. R., Lerario, A. M., Vainchtein, I. D., Brouwer, N., Sola, P. R., Veras, M. M., Pereira, T. F., Leite, R. E. P., *et al.* (2017) 'Transcriptomic analysis of purified human cortical microglia reveals age-associated changes', *Nature Neuroscience*, 20(8), pp. 1162–1171. doi: 10.1038/nn.4597.

Gu, H., Yang, X., Mao, X., Xu, E., Qi, C., Wang, H., Brahmachari, S., York, B., Sriparna, M., *et al.* (2021) 'Lymphocyte Activation Gene 3 (Lag3) Contributes to α-Synucleinopathy in α-Synuclein Transgenic Mice ', *Frontiers in Cellular Neuroscience* , p. 61. Available at: https://www.frontiersin.org/article/10.3389/fncel.2021.656426.

Guo, W., Zhou, M., Qiu, J., Lin, Y., Chen, X., Huang, S., Mo, M., Liu, H., Peng, G., *et al.* (2019) 'Association of LAG3 genetic variation with an increased risk of PD in Chinese female population', *Journal of Neuroinflammation*, 16(1). doi: 10.1186/s12974-019-1654-6.

Hannier, S. and Triebel, F. (1999) 'The MHC class II ligand lymphocyte activation gene-3 is co-distributed with CD8 and CD3-TCR molecules after their engagement by mAb or peptide-MHC class I complexes', *International Immunology*, 11(11), pp. 1745–1752. doi: 10.1093/intimm/11.11.1745.

Hayashita-Kinoh, H., Yamada, M., Yokota, T., Mizuno, Y. and Mochizuki, H. (2006) 'Down-regulation of α-synuclein expression can rescue dopaminergic cells from cell death in the substantia nigra of Parkinson's disease rat model', *Biochemical and Biophysical Research Communications*, 341(4), pp. 1088–1095. doi: 10.1016/j.bbrc.2006.01.057.

Hruska-Plochan, M., Hembach, K. M., Ronchi, S., Maniecka, Z., Hock, E.-M., Laferriere, F., Sahadevan, S., Hoop, V., Delvendahl, I., *et al.* (2021) 'Single Cell Transcriptomics of Aging Human Neural Networks with Induced TDP-43 Pathology Predicts New Protein Markers of Frontotemporal Dementia', *In preparation*.

Huard, B., Gaulard, P., Faure, F., Hercend, T. and Triebel, F. (1994) 'Cellular expression and tissue distribution of the human LAG-3-encoded protein, an MHC class II ligand', *Immunogenetics*, 39(3), pp. 213–217. doi: 10.1007/BF00241263.

Huard, B., Mastrangeli, R., Prigent, P., Bruniquel, D., Donini, S., El-Tayar, N., Maigret, B., Dréano, M. and Triebel, F. (1997) 'Characterization of the major histocompatibility complex class II binding site on LAG-3 protein', *Proceedings of the National Academy of Sciences of the United States of America*, 94(11), pp. 5744–5749. doi: 10.1073/pnas.94.11.5744.

Jankovic, J. (2017) 'Movement disorders in 2016: Progress in Parkinson disease and other movement disorders', *Nature Reviews Neurology*. Nature Publishing Group, pp. 76–78. doi: 10.1038/nrneurol.2016.204.

Jucker, M. and Heikenwalder, M. (2016) 'Immune receptor for pathogenic α-synuclein', *Science*. American Association for the Advancement of Science, pp. 1498–1499. doi: 10.1126/science.aai9377.

Jucker, M. and Walker, L. C. (2018) 'Propagation and spread of pathogenic protein assemblies in neurodegenerative diseases', *Nature Neuroscience*. Nature Publishing Group, pp. 1341–1349. doi: 10.1038/s41593-018-0238-6.

Kara, E., Marks, J. D. and Aguzzi, A. (2018) 'Toxic Protein Spread in Neurodegeneration: Reality versus Fantasy', *Trends in Molecular Medicine*. Elsevier Ltd, pp. 1007–1020. doi: 10.1016/j.molmed.2018.09.004.

Lichtenegger, F. S., Rothe, M., Schnorfeil, F. M., Deiser, K., Krupka, C., Augsberger, C., Schluter, M., Neitz, J. and Subklewe, M. (2018) 'Targeting LAG-3 and PD-1 to Enhance T Cell Activation by Antigen-Presenting Cells', *Front Immunol*, 9, p. 385. doi: 10.3389/fimmu.2018.00385.

Lim, M., Ye, X., Piotrowski, A. F., Desai, A. S., Ahluwalia, M. S., Walbert, T., Fisher, J. D., Desideri, S., Nabors, L. B., *et al.* (2020) 'Updated safety phase I trial of anti-LAG-3 alone and in combination with anti-PD-1 in patients with recurrent GBM.', *Journal of Clinical Oncology*, 38(15_suppl), p. 2512. doi: 10.1200/JCO.2020.38.15_suppl.2512.

Liu, Y. and Aguzzi, A. (2019) 'Immunotherapy for neurodegeneration?', *Science*. American Association for the Advancement of Science, pp. 130–131. doi: 10.1126/science.aaw0685.

Liu, Y., Sorce, S., Nuvolone, M., Domange, J. and Aguzzi, A. (2018) 'Lymphocyte activation gene 3 (Lag3) expression is increased in prion infections but does not modify disease progression', *Scientific Reports*, 8(1). doi: 10.1038/s41598-018-32712-8.

Luk, K. C., Song, C., O'Brien, P., Stieber, A., Branch, J. R., Brunden, K. R., Trojanowski, J. Q. and Lee, V. M. Y. (2009) 'Exogenous α-synuclein fibrils seed the formation of Lewy body-like intracellular inclusions in cultured cells', *Proceedings of the National Academy of Sciences of the United States of America*, 106(47), pp. 20051–20056. doi: 10.1073/pnas.0908005106.

Lun, A. T. L., McCarthy, D. J. and Marioni, J. C. (2016) 'A step-by-step workflow for low-level analysis of single-cell RNA-seq data with Bioconductor [version 2; peer review: 3 approved, 2 approved with reservations]', *F1000Research*, 5(2122). doi: 10.12688/f1000research.9501.2.

Maçon-Lemaître, L. and Triebel, F. (2005) 'The negative regulatory function of the lymphocyte-

activation gene-3 co-receptor (CD223) on human T cells', *Immunology*, 115(2), pp. 170–178. doi: 10.1111/j.1365-2567.2005.02145.x.

Mao, X., Ou, M. T., Karuppagounder, S. S., Kam, T. I., Yin, X., Xiong, Y., Ge, P., Umanah, G. E., Brahmachari, S., *et al.* (2016) 'Pathological α-synuclein transmission initiated by binding lymphocyte-activation gene 3', *Science*, 353(6307). doi: 10.1126/science.aah3374.

Mattsson, N., Andreasson, U., Persson, S., Arai, H., Batish, S. D., Bernardini, S., Bocchio-Chiavetto, L., Blankenstein, M. A., Carrillo, M. C., *et al.* (2011) 'The Alzheimer's Association external quality control program for cerebrospinal fluid biomarkers', *Alzheimer's and Dementia*, 7(4). doi: 10.1016/j.jalz.2011.05.2243.

Miyazaki, T., Dierich, A., Benoist, C. and Mathis, D. (1996) 'Independent modes of natural killing distinguished in mice lacking Lag3.', *Science (New York, N.Y.)*, 272(5260), pp. 405–408. doi: 10.1126/science.272.5260.405.

Mullin, S. and Schapira, A. H. V. (2015) 'Pathogenic Mechanisms of Neurodegeneration in Parkinson Disease', *Neurologic Clinics*. W.B. Saunders, pp. 1–17. doi: 10.1016/j.ncl.2014.09.010.

Myers, A. J., Gibbs, J. R., Webster, J. A., Rohrer, K., Zhao, A., Marlowe, L., Kaleem, M., Leung, D., Bryden, L., *et al.* (2007) 'A survey of genetic human cortical gene expression', *Nature Genetics*, 39(12), pp. 1494–1499. doi: 10.1038/ng.2007.16.

Nguyen, L. T. and Ohashi, P. S. (2015) 'Clinical blockade of PD1 and LAG3-potential mechanisms of action', *Nature Reviews Immunology*. Nature Publishing Group, pp. 45–56. doi: 10.1038/nri3790.

Novotny, R., Langer, F., Mahler, J., Skodras, A., Vlachos, A., Wegenast-Braun, B. M., Kaeser, S. A., Neher, J. J., Eisele, Y. S., *et al.* (2016) 'Conversion of synthetic Aβ to In Vivo active seeds and amyloid plaque formation in a hippocampal slice culture model', *Journal of Neuroscience*, 36(18), pp. 5084–5093. doi: 10.1523/JNEUROSCI.0258-16.2016.

Polinski, N. K., Volpicelli-Daley, L. A., Sortwell, C. E., Luk, K. C., Cremades, N., Gottler, L. M., Froula, J., Duffy, M. F., Lee, V. M. Y., *et al.* (2018) 'Best practices for generating and using alpha-synuclein pre-formed fibrils to model Parkinson's disease in rodents', *Journal of Parkinson's Disease*, 8(2), pp. 303–322. doi: 10.3233/JPD-171248.

Van Der Putten, H., Wiederhold, K. H., Probst, A., Barbieri, S., Mistl, C., Danner, S., Kauffmann, S., Hofele, K., Spooren, W. P. J. M., *et al.* (2000) 'Neuropathology in mice expressing human α-synuclein', *Journal of Neuroscience*, 20(16), pp. 6021–6029. doi: 10.1523/jneurosci.20-16-06021.2000.

Rohatgi, A., Massa, R. C., Gooding, W. E., Bruno, T. C., Vignali, D. and Kirkwood, J. M. (2020) 'A phase

II study of anti-PD1 monoclonal antibody (Nivolumab) administered in combination with anti-LAG3 monoclonal antibody (Relatlimab) in patients with metastatic melanoma naive to prior immunotherapy in the metastatic setting.', *Journal of Clinical Oncology*, 38(15_suppl), pp. TPS10085–TPS10085. doi: 10.1200/JCO.2020.38.15_suppl.TPS10085.

De Rossi, P., Nomura, T., Andrew, R. J., Masse, N. Y., Sampathkumar, V., Musial, T. F., Sudwarts, A., Recupero, A. J., Le Metayer, T., *et al.* (2020) 'Neuronal BIN1 Regulates Presynaptic Neurotransmitter Release and Memory Consolidation', *Cell Reports*, 30(10), pp. 3520-3535.e7. doi: 10.1016/j.celrep.2020.02.026.

Russo, I., Kaganovich, A., Ding, J., Landeck, N., Mamais, A., Varanita, T., Biosa, A., Tessari, I., Bubacco, L., *et al.* (2019) 'Transcriptome analysis of LRRK2 knock-out microglia cells reveals alterations of inflammatory- and oxidative stress-related pathways upon treatment with α-synuclein fibrils', *Neurobiology of Disease*, 129, pp. 67–78. doi: 10.1016/j.nbd.2019.05.012.

Saez-Atienzar, S., Bandres-Ciga, S., Langston, R. G., Kim, J. J., Choi, S. W., Reynolds, R. H., Abramzon, Y., Dewan, R., Ahmed, S., *et al.* (2021) 'Genetic analysis of amyotrophic lateral sclerosis identifies contributing pathways and cell types', *Science Advances*, 7(3). doi: 10.1126/sciadv.abd9036.

Scheckel, C. and Aguzzi, A. (2018) 'Prions, prionoids and protein misfolding disorders', *Nature Reviews Genetics*. Nature Publishing Group, pp. 405–418. doi: 10.1038/s41576-018-0011-4.

Scheidt, T., Łapińska, U., Kumita, J. R., Whiten, D. R., Klenerman, D., Wilson, M. R., Cohen, S. I. A., Linse, S., Vendruscolo, M., *et al.* (2019) 'Secondary nucleation and elongation occur at different sites on Alzheimer's amyloid-β aggregates', *Science Advances*, 5(4), p. eaau3112. doi: 10.1126/sciadv.aau3112.

Schelle, J., Häsler, L. M., Göpfert, J. C., Joos, T. O., Vanderstichele, H., Stoops, E., Mandelkow, E. M., Neumann, U., Shimshek, D. R., *et al.* (2017) 'Prevention of tau increase in cerebrospinal fluid of APP transgenic mice suggests downstream effect of BACE1 inhibition', *Alzheimer's and Dementia*, 13(6), pp. 701–709. doi: 10.1016/j.jalz.2016.09.005.

Schneider, M. M., Gautam, S., Herling, T. W., Andrzejewska, E., Krainer, G., Miller, A. M., Peter, Q. A. E., Ruggeri, F. S., Vendruscolo, M., *et al.* (2020) 'The Hsc70 Disaggregation Machinery Removes Monomer Units Directly from α-Synuclein Fibril Ends', *bioRxiv*, p. 2020.11.02.365825. doi: 10.1101/2020.11.02.365825.

Schwartz, M. (2017) 'Can immunotherapy treat neurodegeneration?', *Science*. American Association for the Advancement of Science, pp. 254–255. doi: 10.1126/science.aai8231.

Shrivastava, A. N., Redeker, V., Fritz, N., Pieri, L., Almeida, L. G., Spolidoro, M., Liebmann, T., Bousset,

L., Renner, M., *et al.* (2015) ' α-synuclein assemblies sequester neuronal α3-Na + /K + - ATP ase and impair Na + gradient ', *The EMBO Journal*, 34(19), pp. 2408–2423. doi: 10.15252/embj.201591397.

Stuart, T., Butler, A., Hoffman, P., Hafemeister, C., Papalexi, E., Mauck, W. M., Hao, Y., Stoeckius, M., Smibert, P., *et al.* (2019) 'Comprehensive Integration of Single-Cell Data', *Cell*, 177(7), pp. 1888-1902.e21. doi: 10.1016/j.cell.2019.05.031.

Tasic, B., Menon, V., Nguyen, T. N., Kim, T. K., Jarsky, T., Yao, Z., Levi, B., Gray, L. T., Sorensen, S. A., *et al.* (2016) 'Adult mouse cortical cell taxonomy revealed by single cell transcriptomics', *Nature Neuroscience*, 19(2), pp. 335–346. doi: 10.1038/nn.4216.

Thrupp, N., Sala Frigerio, C., Wolfs, L., Skene, N. G., Fattorelli, N., Poovathingal, S., Fourne, Y., Matthews, P. M., Theys, T., *et al.* (2020) 'Single-Nucleus RNA-Seq Is Not Suitable for Detection of Microglial Activation Genes in Humans', *Cell Reports*, 32(13). doi: 10.1016/j.celrep.2020.108189.

Triebel, F., Jitsukawa, S., Baixeras, E., Roman-Roman, S., Genevee, C., Viegas-Pequignot, E. and Hercend, T. (1990) 'LAG-3, a novel lymphocyte activation gene closely related to CD4', *J Exp Med*. 1990/05/01, 171(5), pp. 1393–1405. doi: 10.1084/jem.171.5.1393.

Uemura, N., Uemura, M. T., Luk, K. C., Lee, V. M. Y. and Trojanowski, J. Q. (2020) 'Cell-to-Cell Transmission of Tau and α-Synuclein', *Trends in Molecular Medicine*. Elsevier Ltd. doi: 10.1016/j.molmed.2020.03.012.

Volpicelli-Daley, L. A., Luk, K. C. and Lee, V. M. Y. (2014) 'Addition of exogenous α-synuclein preformed fibrils to primary neuronal cultures to seed recruitment of endogenous α-synuclein to Lewy body and Lewy neurite-like aggregates', *Nature Protocols*. Nature Publishing Group, pp. 2135–2146. doi: 10.1038/nprot.2014.143.

Volpicelli-Daley, L. A., Luk, K. C., Patel, T. P., Tanik, S. A., Riddle, D. M., Stieber, A., Meaney, D. F., Trojanowski, J. Q. and Lee, V. M. Y. (2011) 'Exogenous α-Synuclein Fibrils Induce Lewy Body Pathology Leading to Synaptic Dysfunction and Neuron Death', *Neuron*, 72(1), pp. 57–71. doi: 10.1016/j.neuron.2011.08.033.

Wang, J., Sanmamed, M. F., Datar, I., Su, T. T., Ji, L., Sun, J., Chen, L. L. L. L., Chen, Y., Zhu, G., *et al.* (2019) 'Fibrinogen-like Protein 1 Is a Major Immune Inhibitory Ligand of LAG-3', *Cell*. 2018/12/26, 176(1–2), pp. 334-347 e12. doi: 10.1016/j.cell.2018.11.010.

Welch, J. D., Kozareva, V., Ferreira, A., Vanderburg, C., Martin, C. and Macosko, E. Z. (2019) 'Single-Cell Multi-omic Integration Compares and Contrasts Features of Brain Cell Identity', *Cell*, 177(7), pp. 1873-1887.e17. doi: 10.1016/j.cell.2019.05.006.

Wong, Y. C. and Krainc, D. (2017) 'α-synuclein toxicity in neurodegeneration: Mechanism and therapeutic strategies', *Nature Medicine*. Nature Publishing Group, pp. 1–13. doi: 10.1038/nm.4269.

Wood, H. (2016) 'Parkinson disease: LAG3 facilitates cell-to-cell spread of α-synuclein pathology', *Nature Reviews Neurology*. Nature Publishing Group, p. 678. doi: 10.1038/nrneurol.2016.164.

Workman, C. J., Rice, D. S., Dugger, K. J., Kurschner, C. and Vignali, D. A. (2002) 'Phenotypic analysis of the murine CD4-related glycoprotein, CD223 (LAG-3)', *Eur J Immunol*, 32(8), pp. 2255–2263. doi: 10.1002/1521-4141(200208)32:8<2255::AID-IMMU2255>3.0.CO;2-A.

Workman, C. J., Wang, Y., El Kasmi, K. C., Pardoll, D. M., Murray, P. J., Drake, C. G. and Vignali, D. A. A. (2009) 'LAG-3 regulates plasmacytoid dendritic cell homeostasis', *J Immunol*, 182(4), pp. 1885–1891. doi: 10.4049/jimmunol.0800185.

Wright, M. A., Aprile, F. A., Bellaiche, M. M. J., Michaels, T. C. T., Müller, T., Arosio, P., Vendruscolo, M., Dobson, C. M. and Knowles, T. P. J. (2018) 'Cooperative Assembly of Hsp70 Subdomain Clusters', *Biochemistry*, 57(26), pp. 3641–3649. doi: 10.1021/acs.biochem.8b00151.

Zhang, Y., Chen, K., Sloan, S. A., Bennett, M. L., Scholze, A. R., O'Keeffe, S., Phatnani, H. P., Guarnieri, P., Caneda, C., *et al.* (2014) 'An RNA-sequencing transcriptome and splicing database of glia, neurons, and vascular cells of the cerebral cortex', *Journal of Neuroscience*, 34(36), pp. 11929–11947. doi: 10.1523/JNEUROSCI.1860-14.2014.

Zhang, Y., Sloan, S. A., Clarke, L. E., Caneda, C., Plaza, C. A., Blumenthal, P. D., Vogel, H., Steinberg, G. K., Edwards, M. S. B., *et al.* (2016) 'Purification and Characterization of Progenitor and Mature Human Astrocytes Reveals Transcriptional and Functional Differences with Mouse', *Neuron*, 89(1), pp. 37–53. doi: 10.1016/j.neuron.2015.11.013.

Acknowledgments

Rita Moos, Leyla Batkitar, Lidia Madrigal, and Petra Schwarz provided technical assistance and help with mouse breeding, and Julie Domange, Marigona Imeri, Dezirae Schneider, and Lisa Caflisch assisted with lab management.

Funding

Institutional core funding by the University of Zurich and the University Hospital of Zurich to AA, as well as Driver Grant 2017DRI17 of the Swiss Personalized Health Network and an Advanced Grant of the European Research Council and a Distinguished Scientist Award of the Nomis Foundation to AA. The research presented in this manuscript has received funding from the European Research Council (ERC) under the European Union's Seventh Framework Programme (FP7/2007-2013) through the ERC grant PhysProt (agreement no. 337969) and under European Union's Horizon 2020 research and innovation programme (ETN grant 674979-NANOTRANS) (MMS, TWH, NSM, TPJK). MP gratefully acknowledges the support by the National Centre for Competence in Research (NCCR) RNA & Disease (51NF40-182880) and Project Grant 310030_192650 funded by the Swiss National Science Foundation.

Author contributions

Conducted experiments: MHP, TE, MB, ME, EDC, PDR, ET, AGG, AK, RGL, LMH, TWH, MMS. Contributed reagents/materials: KL, RM, PJK, RR, MA, DH. Conceived the study: AA, ME. Supervised the study and provided crucial advice: AA, MJ, MP, MRC, TPJK, SH. Wrote the manuscript: AA, ME, EDC, MHP.

Competing interests

AA is a member of the board of directors of Mabylon AG which has funded antibody-related work in the Aguzzi lab in the past. All other authors declare no competing interests.

Data and materials availability

The raw data underlying this study will be made available upon request.

Supplementary Figures

Fig. S1. **A**. Expression levels of cellular markers and control genes in human NSC-derived neuronal cultures assessed by scRNAseq. **B**. Western Blotting of brain homogenates from LAG3 KO and WT mice, with activated murine T cells as controls. Anti-LAG3 antibody LSB15026 was used.

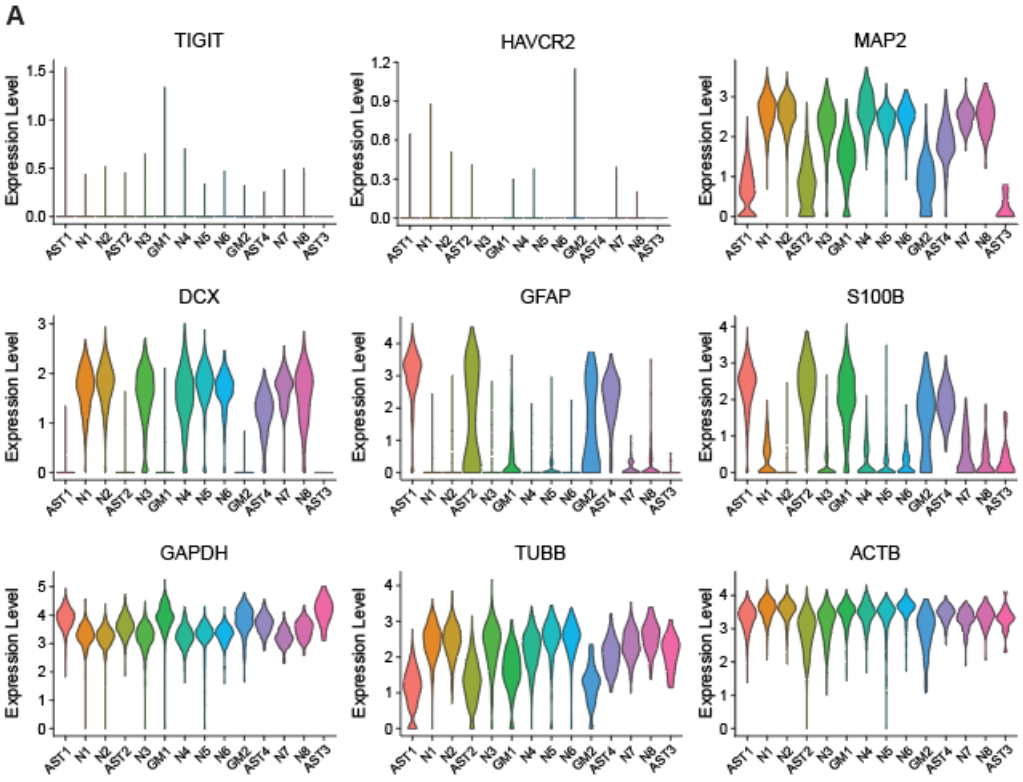

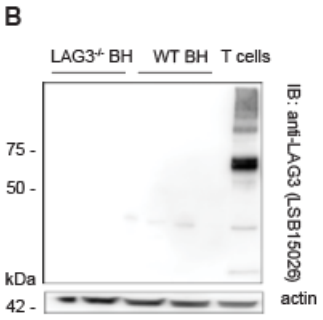

Emmenegger et al. Figure S1

Fig. S2. **A**. and **B**. IP-enrichment of murine brain homogenates (A) and cultures (B). The enrichment was performed with anti-LAG3 antibody (4-10-C9) and the immunoblot was done with LSB15026. **C**. Uniform Manifold Approximation and Projection (UMAP) visualization of cell clusters identified by scRNAseq of 76'305 cells derived from the mouse midbrain and striatum, with major cell types labelled. **D**. Feature plot showing distribution of Lag3 transcripts in the identified mouse cell types from the midbrain and striatum area. **E**. Lag3 transcript levels after striatal injections of PBS or LPS. LPS treatment decreases detectable transcripts, while the basal expression is already extremely low.

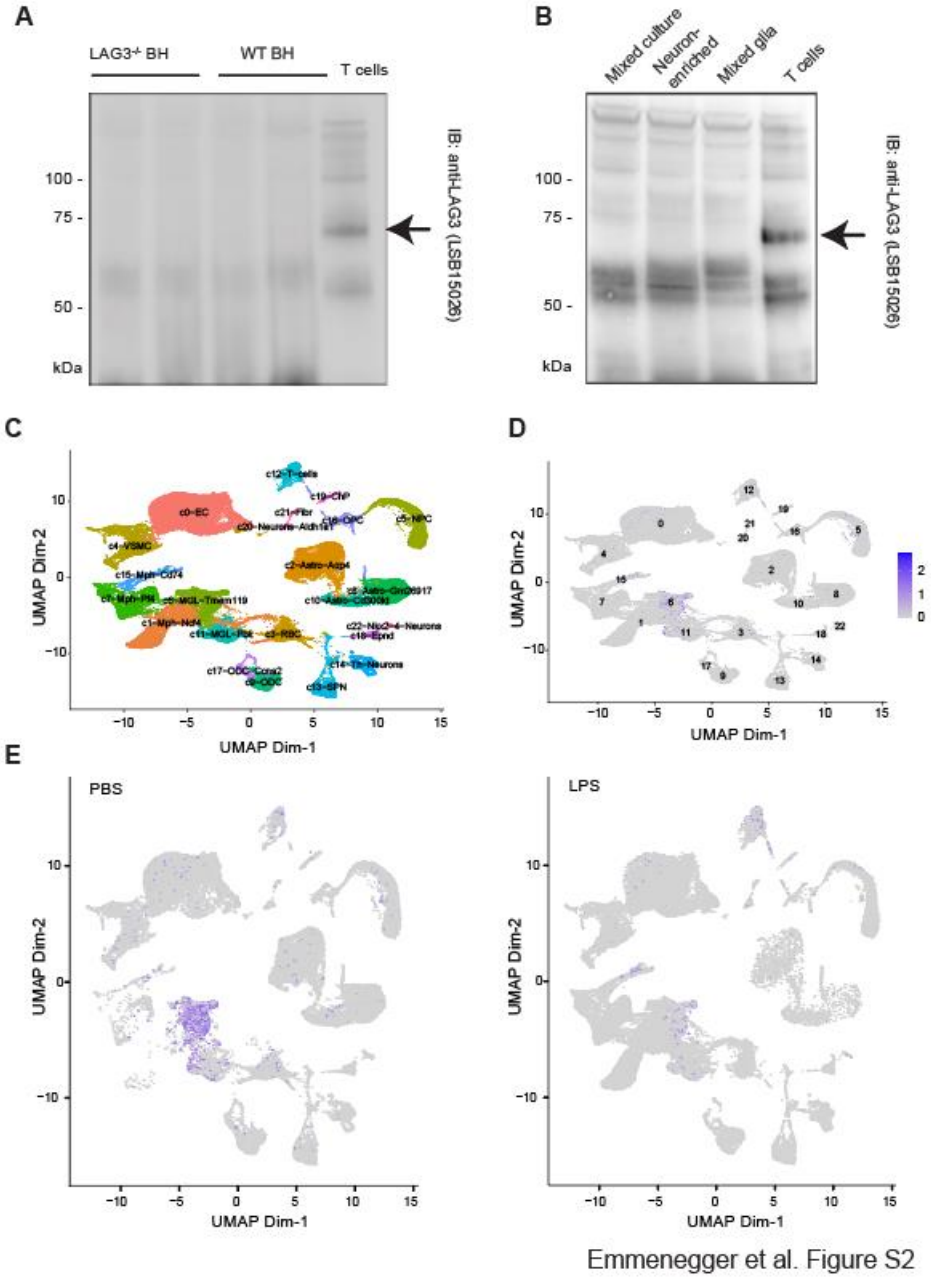

Emmenegger et al. Figure S2

Fig. S3. **A**. Serially diluted ASC filaments, directly bound to the plate, were recognized using an anti-ASC antibody in indirect ELISA.

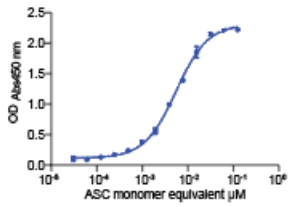

Emmenegger et al. Figure S3

1065

Fig. S4. **A**. Neurons (MAP2+ cells) in human neural cultures express α-synuclein (MJFR1). **B**. Human neural cultures transduced with Auto-hLAG3 LVs do not show any positivity for LAG3 (17B4) in DOX OFF condition. **C**. Upon inducing the expression of hLAG3 (DOX ON condition), transgenic neurons display LAG3 positivity (17B4), while non-transduced cells remain negative. Scale bars 25µm.

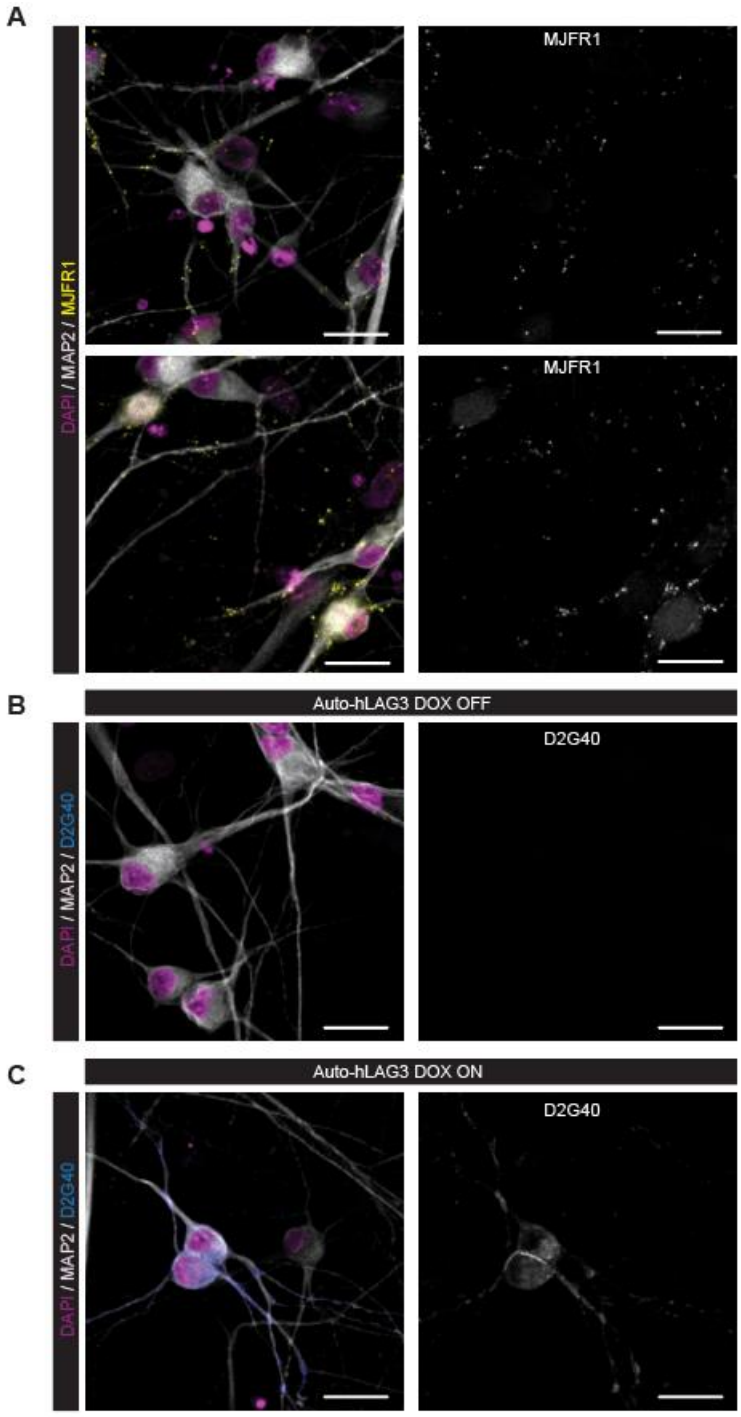

Fig. S5. **A**. Levels of α-synuclein in murine CSF quantified using SIMOA. No significantly altered expression levels of human α-synuclein could be identified. Shown are all dots as well as their means and the standard deviation. Average age of A53T α-synuclein TG LAG3$^{+/+}$ (LAG3 WT; n=7) was 9.1 months; 8.0 months for A53T α-synuclein TG LAG3$^{-/-}$ (LAG3 KO; n=7).